1966-05

A photoelastic investigation of stresses in two different pipe fittings

Davies, Richard Everett

Monterey, California. U.S. Naval Postgraduate School

A PHOTOELASTIC INVESTIGATION OF STRESSES IN TWO DIFFERENT PIPE FITTINGS

RICHARD EVERETT DAVIES

A PHOTOELASTIC INVESTIGATION OF STRESSES IN TWO DIFFERENT PIPE FITTINGS

by

Richard Everett Davies
Lieutenant, United States Navy
B.S., United States Naval Academy, 1958

Submitted in partial fulfillment
for the degree of

MASTER OF SCIENCE IN MECHANICAL ENGINEERING

from the

UNITED STATES NAVAL POSTGRADUATE SCHOOL
May 1966

ABSTRACT

Photoelastic methods using frozen stresses are very useful for experimentally determining stress distributions in bodies having complicated geometries for which no analytical solution is known. The method is applied to cylindrical pipe fittings having discontinuities and subjected to hydrostatic internal pressure loading. The equipment used, the method of model construction and the calibration of the model material are described. Two models having different geometries are tested and the results are compared with theory and with each other.

TABLE OF CONTENTS

LIST OF ILLUSTRATIONS

NOMENCLATURE

English Letter Symbols

a	inside radius
a_m	mean radius
Å	Ångstrom units
b	outside radius
E	modulus of elasticity
f	photoelastic material fringe constant for stress
h	wall thickness or beam height
I	moment of inertia (second moment of area) about centroidal axis
M	moment
N	fringe order
n	total number of fringes present
P	force
p_i	internal pressure
r	radius, radial cylindrical co-ordinate
t	thickness of a slice or beam
z	longitudinal distance, longitudinal cylindrical co-ordinate

Greek Letter Symbols

β	parameter used in shall bending theory
θ	angular position, angular cylindrical co-ordinate
μ	Poisson's ratio
π	the constant 3.14159.....
σ	stress (general)

σ_1, σ_2	general normal stresses
σ_θ	circumferential normal stress
σ_r	radial normal stress
σ_z	longitudinal normal stress

Section 1. Introduction

The use of photoelastic techniques to study three-dimensional models is not new; "stress freezing" has been known and applied for about thirty years. In recent years these methods have received renewed interest from many investigators because of the relative ease with which useful results can be obtained for problems with complicated geometries or having complex systems of loading, and for which analytical solutions are cumbersome or are not known.

It was decided to investigate stress distributions in a cylindrical body of revolution containing discontinuities. The specific geometry chosen was that of a straight coupling joining two short sections of pipe. The loading selected was internal hydrostatic pressure. This problem was selected because it has rather wide engineering applications and because failures often occur near the joints in piping systems.

Section 2. Model Design

The exact geometry selected was that of a cylindrical, socket ended straight coupling joining two short sections of pipe. The pipe size corresponded to 1-½ inch ASTM Schedule 80 pipe having an inside diameter of 1.500 inch and an outside diameter of 1.900 inch. The matching coupling was 2-3/4 inches long, with an inside diameter of 1.500 inch and an outside diameter of 2.200 inches. The sockets were specified to be one-half inch deep, with an inside diameter appropriate to provide a slightly loose sliding fit with the pipe, or about 1.905 inches. The arrangement of the components is shown in figures 1 and 2.

One model followed the above plan exactly; it will hereafter be referred to as Model II. The other model was modified by the addition

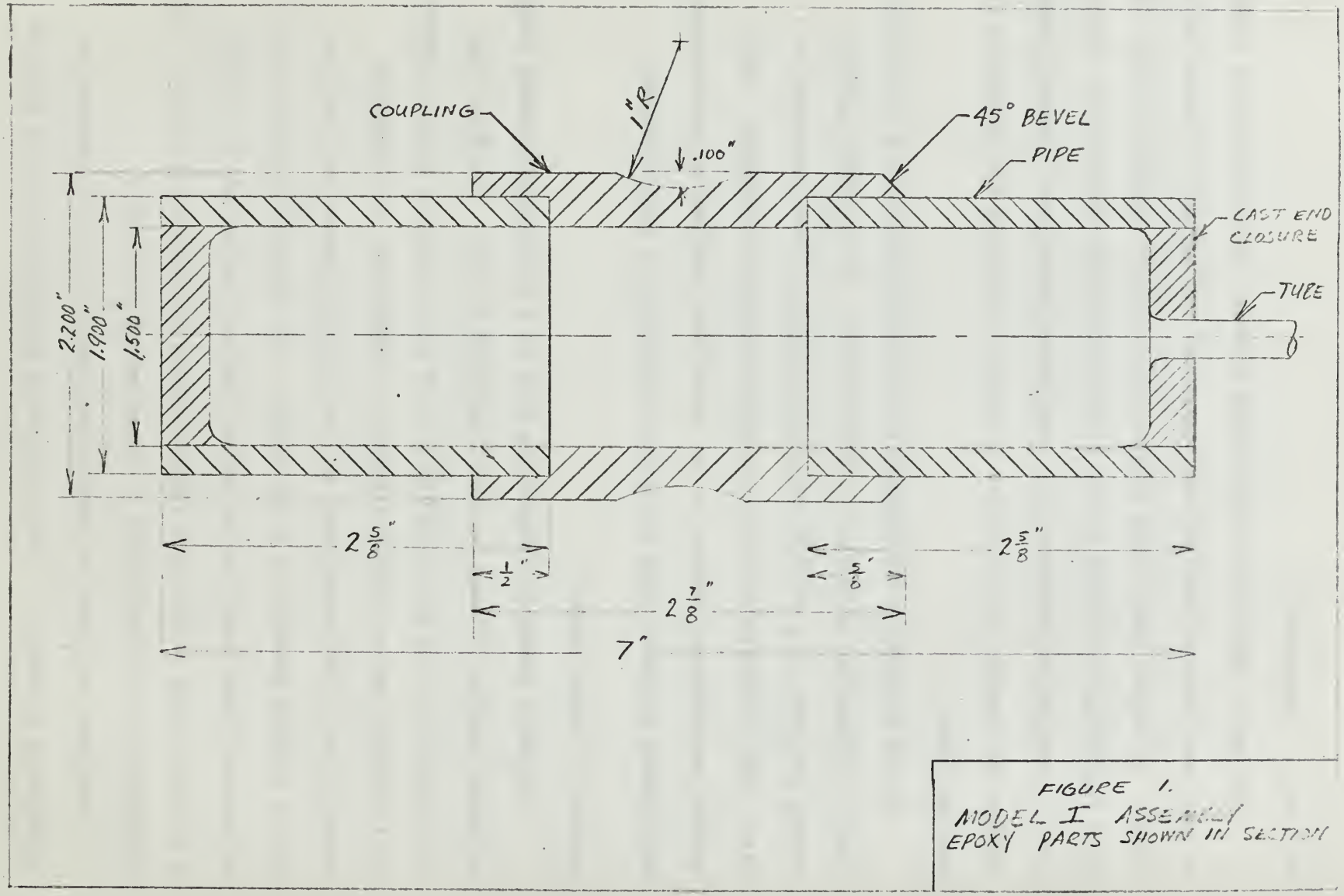

Figure 1. Model I Assembly Drawing.

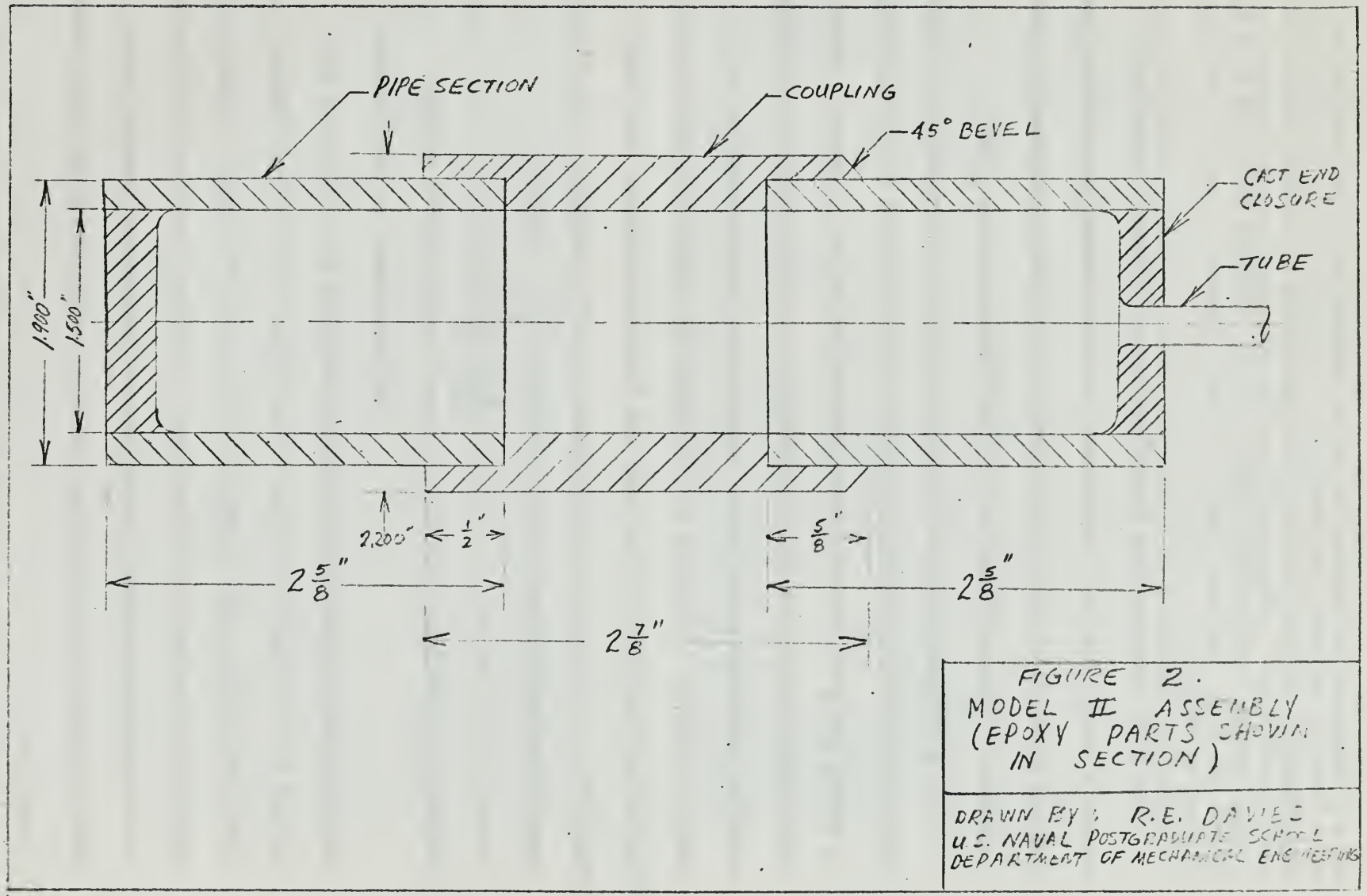

Figure 2. Model II Assembly Drawing.

of a circumferential groove cut in the midsection of the coupling to a root diameter of 2.000 inches. This groove had a circular profile of 1 inch radius. This modified model will be referred to in the text and figures as Model I.

The pipe sections were jointed to the couplings by cementing to create a joint similar in appearance to silver brazed pipe joints. One end was modified slightly by the addition of a 45 degree bevel in order to simulate a corner filled with a non-flowing brazing alloy.

The dimensions selected for the models were convenient to fit the oven and the polariscope field of view. An additional factor considered in sizing the pipe stubs was the presence of the end closures. These were almost rigid constraints on the pipe when the loading was applied, creating localized disturbances consisting of bending moments and shearing forces. According to the theory for bending of cylindrical shells as presented by Timoshenko and Woinowsky-Krieger, the disturbances die out with increasing distance along the cylinder. The theory states that effects are negligible for $z > \frac{\pi}{\beta}$, where

$$\beta^4 = \frac{3(1-\mu^2)}{a_m^2 h^2}$$

and where μ = Poisson's ratio, a_m = mean radius of the cylinder

h = wall thickness of the cylinder

For the selected pipe dimensions, this value of z is $\frac{\pi}{2.98}$, or 1.05 inches. [5][1] Therefore, it was inferred that the end disturbances would not extend to the vicinity of the joint. The "safe" length calculated here can only be an estimate inasmuch as the theory was developed for axi-symmetric shells in which the original stress system was bi-axial, containing only membrane stresses, and in which the final stress

[1] Numbers in square brackets refer to publications listed in the bibliography.

system created by the localized disturbances was composed of shell bending stresses super-imposed upon the original system. The selected geometry has a triaxial stress system and other deviations from the assumptions of the above theory; these are more fully described in Section 7.

Section 3. Model Construction

It was decided to machine the model components from commercially cast stock in order to avoid the difficulties associated with casting. The material selected for the model components was Hysol CP5-4290 cast epoxy in rod and tube form. The matching cement used for assembly of the components was Hysol R9-2039 liquid resin and H2-3475 hardener. These are stock items available from Hysol Corporation, 1100 Seneca Avenue, Olean, New York. The manufacturer's technical data for Hysol 4290 is shown in Appendix I, page 46.

The pipe sections were machined from two inch diameter tubing; little machining was required. The coupling, however, had to be made from three inch rod stock. This was a straightforward but lengthy process because epoxy must be machined using light cuts to avoid excessive heat generation. (Figure 3 shows the rough stock, two pipe sections, two couplings and two calibration specimens.)

The pipe and coupling sections were joined using the liquid resin and hardener mixed in the proportion of two parts resin to one part hardener, by weight. It was applied liberally, squeezed to force air out, and the excess was wiped from the inner and outer surfaces of the assembly. Both end closures were formed by casting the liquid resin and hardener mixture directly into the open ends of the assembly, one end at a time, using aluminum foil molds. A short section of flared

copper tubing was molded into place in one end closure in order to provide a pressurizing connection for loading the model. A typical completed assembly is shown in figure 4.

All work with the cement required that the mating surfaces be thoroughly degreased. This cleaning was accomplished by dipping in dry cleaning solvent, drying in air, and finally wiping with acetone. After the surfaces had been prepared, the required quantity of cement was mixed, avoiding introduction of air bubbles as much as possible. Pot life after mixing was short--about fifteen minutes. The resin-hardener mixture reacted exothermically with a temperature rise dependent upon the quantity of mixture present in bulk. Thick sections heated themselves enough to accelerate the curing process; curing was complete in about an hour. Thin sections, however, required an overnight cure at room temperature, or about one hour at 180°F.

Section 4. Material Calibration

Several methods of calibration may be employed in stress freezing. The method selected was to use a beam in pure bending as described in Handbook of Experimental Stress Analysis. [3] This type of specimen has a disadvantage of requiring fairly large pieces of stock, but it could be easily made, was easily loaded in available fixtures, could be tested in the same container with a model, and provided a number of data points with a single test.

The length of the calibration beams was limited by the inside diameter of the oil container in which the beams were suspended for the stress freezing cycle. The beam height was selected to avoid the possibility of lateral buckling. Burke suggested a height of one-half

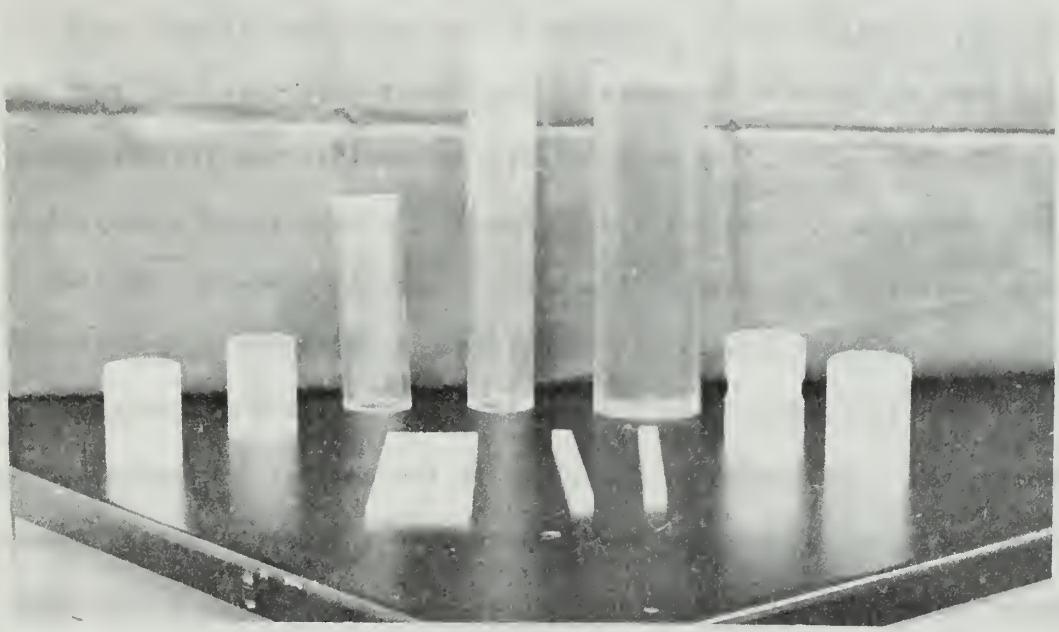

Figure 3. Model Materials.

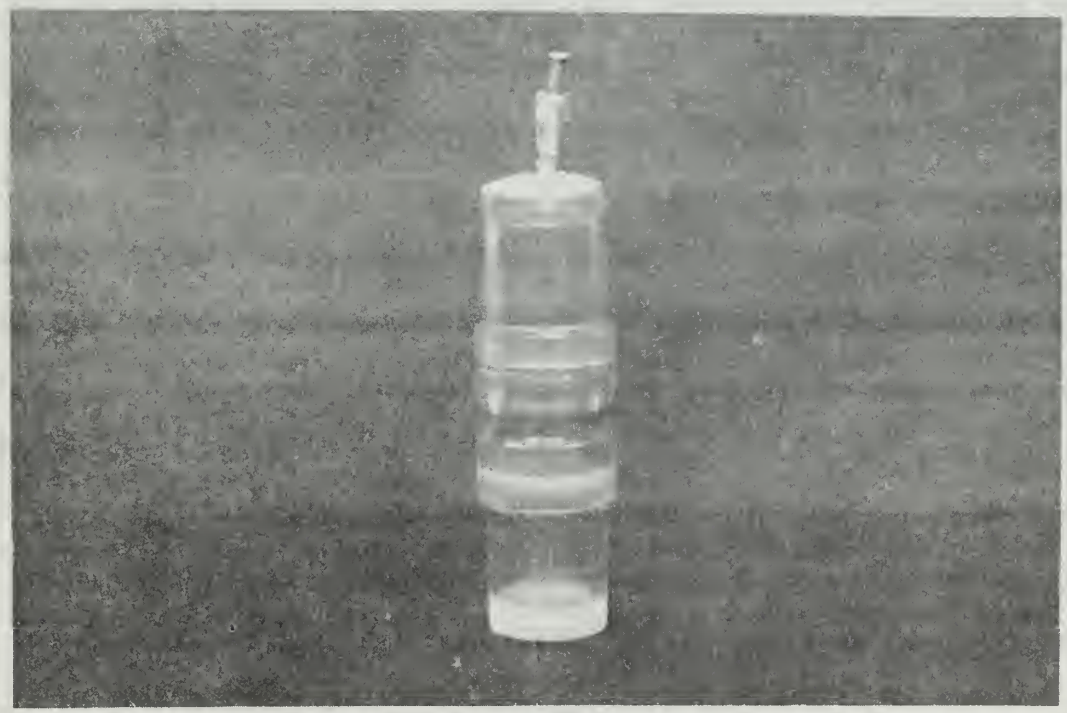

Figure 4. Model I Assembled.

inch. [1] This size was used for this project.

The required specimens were fabricated by first bandsawing two slabs about one-third inch thick from an eight inch length of the three inch diameter epoxy rod. The slabs were machined with a fly cutter to obtain flat, parallel sides. Specimen blanks were cut slightly oversize and both surfaces were sanded by hand until thickness variation was within .001 inch. The holes were drilled, a template was attached, and the final machining of the edges was done with a high speed rotary file.

The drawing of the calibration beam, Figure 5, shows the nominal dimensions. The exact dimensions of height and thickness were determined for each individual specimen by measurement with a micrometer caliper and were tabulated for later use in the calibration calculations.

Each calibration specimen was subjected to a separate stress freezing cycle while it was immersed in mineral oil contained in a tank within the oven. The calibration specimen was either alone or it accompanied one of the models being tested. The reason for this arrangement was to insure that the calibration specimen followed the same temperature program as the model in order to obtain a material fringe value best representing the model material.

The gravitational body force on a calibration beam is small. A Specimen submerged in oil experiences an upward buoyant force which tends to reduce the effect of the body force still further, thus serving to reduce the error incurred by ignoring the additional bending moment caused by this force. A check calculation (Appendix I) shows that the error resulting from neglecting the apparent weight of the calibration beam is about one per cent. A similar effect was of course acting on the

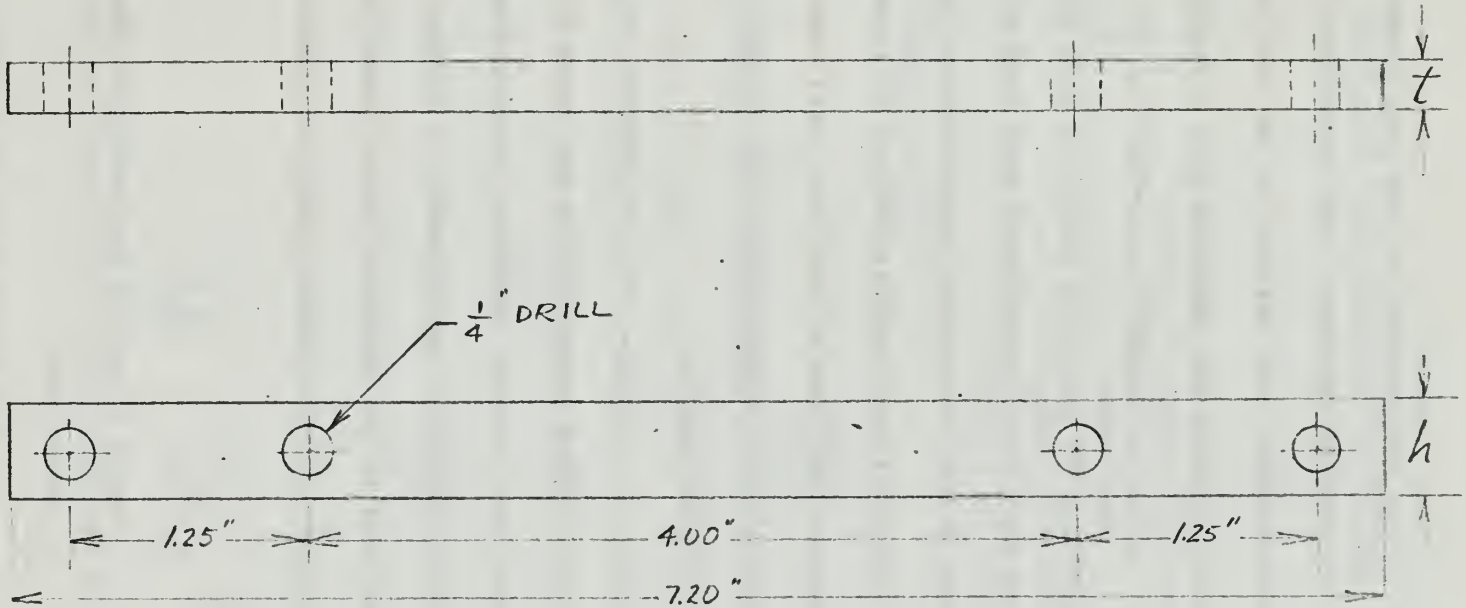

SPECIMEN	h IN.	t IN.
1	NOT	USED
2	.507	.239
3	.509	.237
4	.500	.243
5	.521	.201

FIGURE 5. CALIBRATION SPECIMEN

Figure 5. Calibration Specimen Drawing.

calibration loading weights; this was taken into account simply by weighing them while they were immersed in hot oil to closely approximate the test conditions.

A scale factor for fringe measurements on the photographs of the fringe patterns of the calibration specimens was established individually for each beam. Reference marks were scribed on the side to be photographed and the separation distance was measured with a tool-maker's microscope. Measurement of the corresponding distance on the fringe photograph allowed computation of the scale factor in each case.

Both light field and dark field photographs were made of the isochromatic fringe patterns in each beam using monochromatic light with a wavelength of 5461 Å. The resulting negatives were 2.07 times actual size, but further enlargement was done so that the total magnification of the final prints was about five times actual size in order to facilitate measurement of the fringe spacing.

A plot of fringe order vs. distance from the neutral axis of the beam was made; then a best fitting straight line was drawn through these points. The intercepts at the ordinate distances representing the upper and lower edges of the beam yielded a total number of fringes corresponding to twice the fringe order at the extreme fibers. Calculations to find f, the material fringe value for stress, were then made. From photoelastic theory: [2]

$$\sigma_1 - \sigma_2 = \frac{Nf}{t} \qquad 4.1$$

where σ_1 and σ_2 are principal stresses at a point, psi

N = fringe order at a point

f = material fringe value for stress, lb/in-fringe

t = model or slice thickness, in.

From the equation for the extreme fiber stress in a beam in pure bending:

$$\sigma = \frac{M h}{2 I} \qquad 4.2$$

where σ = extreme fiber stress

h = beam height

I = moment of inertia of the beam cross section about the neutral axis

From 4.2, since $I = \frac{th^3}{12}$:

$$\sigma = \frac{6M}{t h^2} \qquad 4.3$$

This is a tensile (or compressive) principal stress in the outer fibers. Since the other principal stress is zero for this case, equation 4.1 becomes

$$\frac{6M}{th^2} = \frac{Nf}{t}$$

or

$$f = \frac{6M}{Nh^2} \qquad 4.4$$

Since this N is half the value of n, the number of fringes obtained from the photograph, the final calibration equation is

$$f = \frac{12M}{n h^2} \quad lb/in-fringe \qquad 4.5$$

Figure 6 shows a typical set of calculations for the material fringe value.

The manufacturer quotes an average value of 1.35 $\frac{lb}{in\text{-}fringe}$ for Hysol 4290 at a stress freezing temperature of 270°F. One investigator, Pih, found values of 1.354 and 1.362 lb/in/fringe respectively for two

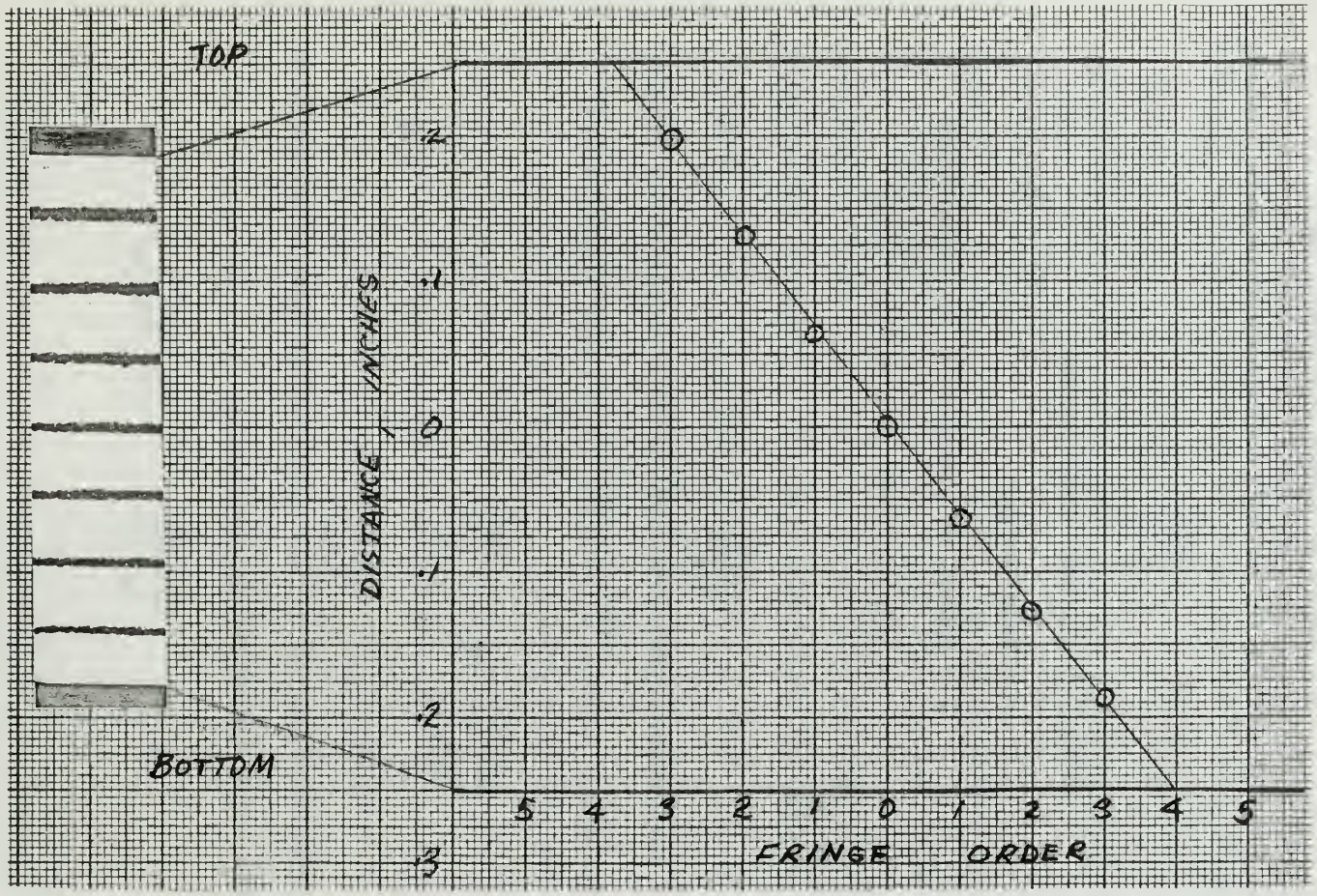

Calibration Specimen No. 4
Scale: 5.83
M = .219 lb-in
Total Fringes = 7.8

$$f = \frac{(12)(.219)}{(.500)(7.8)} = 1.35 \text{ lb/in-fringe}$$

Figure 6. Typical Calibration Calculation

different specimens at a temperature of 280°F. [4] The writer found an average value of 1.37 lb/in-fringe at 280°F. for four specimens from the same piece of stock. This value of the material fringe value was considered reliable and was used in subsequent analyses of the model slices.

According to Dally, the so-called "critical temperature" for stress freezing is not at all critical. [2] A temperature at or above the critical temperature assures rapid response of the material upon application of a load, while temperatures below the critical temperature simply result in a time delay in the response. The stress freezing temperature for this investigation was chosen to be 280°F. in order to be just above the manufacturer's quoted average critical temperature in order to assure rapid response of the models irrespective of the uncertainties in temperature measurement and variations of the actual critical temperature from the average value quoted by the manufacturer.

The writer made all calibration fringe photographs immediately upon removal from the oven in order to avoid time-edge effects. It was found that storage in mineral oil was effective in preventing buildup of time-edge effect stresses.

Section 5. Test Apparatus

The heating and cooling cycle was accomplished in a Central Scientific Company constant temperature oven. Since no time-temperature control was available it was decided to use a temperature set point of the maximum temperature of 280°F., and to allow the oven to heat and cool according to its natural time constant. The empty oven was found to heat and cool too rapidly for stress freezing, but the writer found that

a container holding about one gallon of mineral oil provided even heating of the models and also slowed the heating and cooling rates to acceptable values. See Figure 7 for a typical heating and cooling curve for the oven-oil tank combination. The oil tank was a stainless steel beaker about 8-½ inches in diameter and about 11 inches high. It easily contained the model being tested and a calibration specimen mounted on its loading fixture.

The internal pressure loading of the models was applied by the hydrostatic pressure output from a dead weight gage tester. This instrument, manufactured by Crosby Steam Valve and Gauge Company, was capable of pressures from 0 to 300 psig in 5 psig increments. The pressure actually applied to a model was 10 psig. This pressure provided a number of fringes in the slices large enough to be useful, but the loading was small enough to avoid large deformations of the models.

The connecting piping from the dead weight tester to the model was led into the oven through an existing thermometer hole in the top. Figure 8 shows the oven and the general arrangement of the loading piping before it had been led into the oven. Since the mercury thermometer was removed to make way for the loading piping, a thermocouple junction was placed within the central cavity of the model. The thermocouple wires were led from the model back through the inside of the loading piping to exit immediately outside the oven through a small stuffing box. The thermocouple system is readily visible in Figure 8.

A filling and vent connection was placed in the high point of the piping in order to fill the system with oil and to bleed off any entrapped air. Some slight leakage was present around the thermocouple wires at the first application of pressure. After all the air had been expelled, the

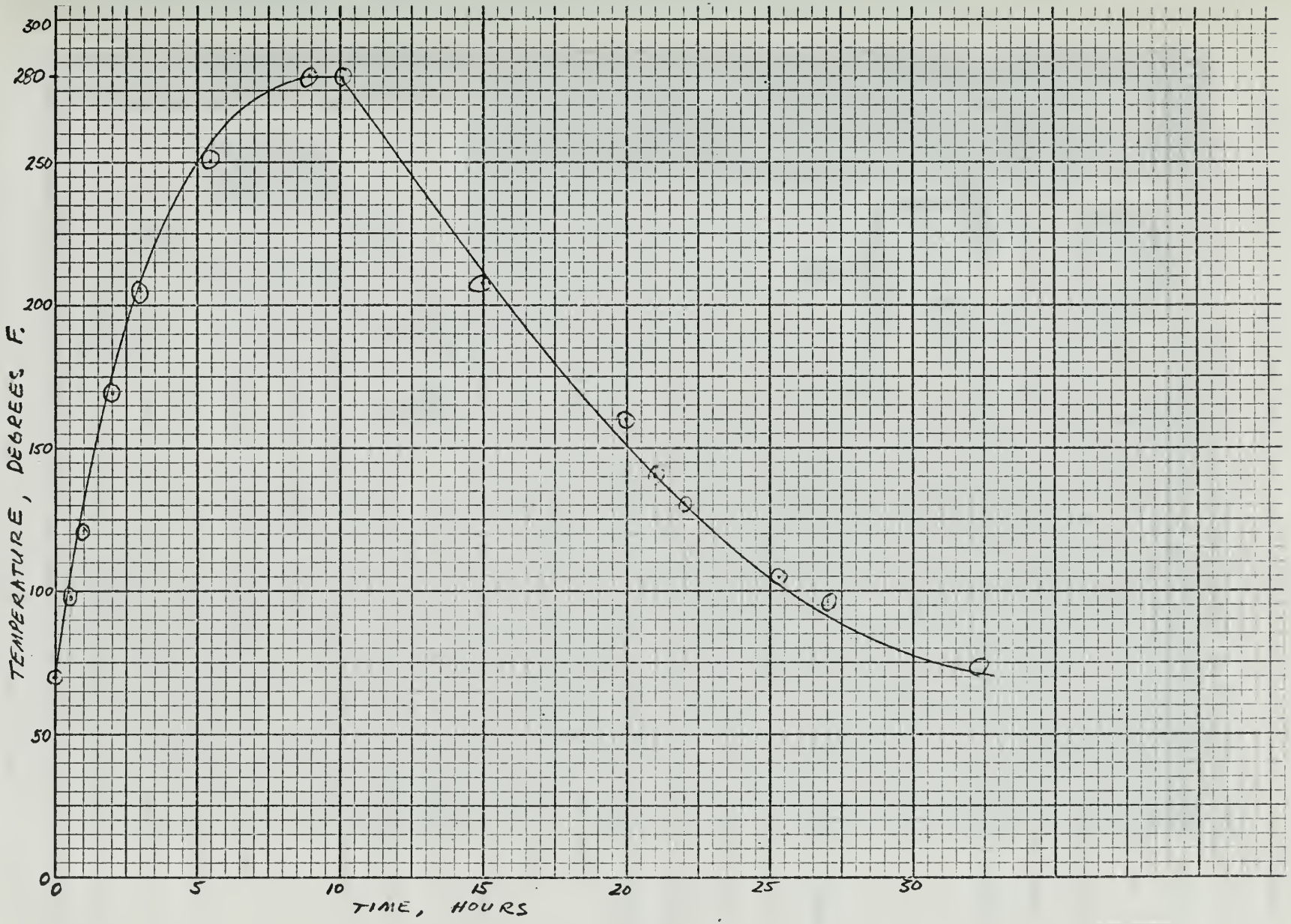

Figure 7. Oven Heating And Cooling Curve For Stress Freezing.

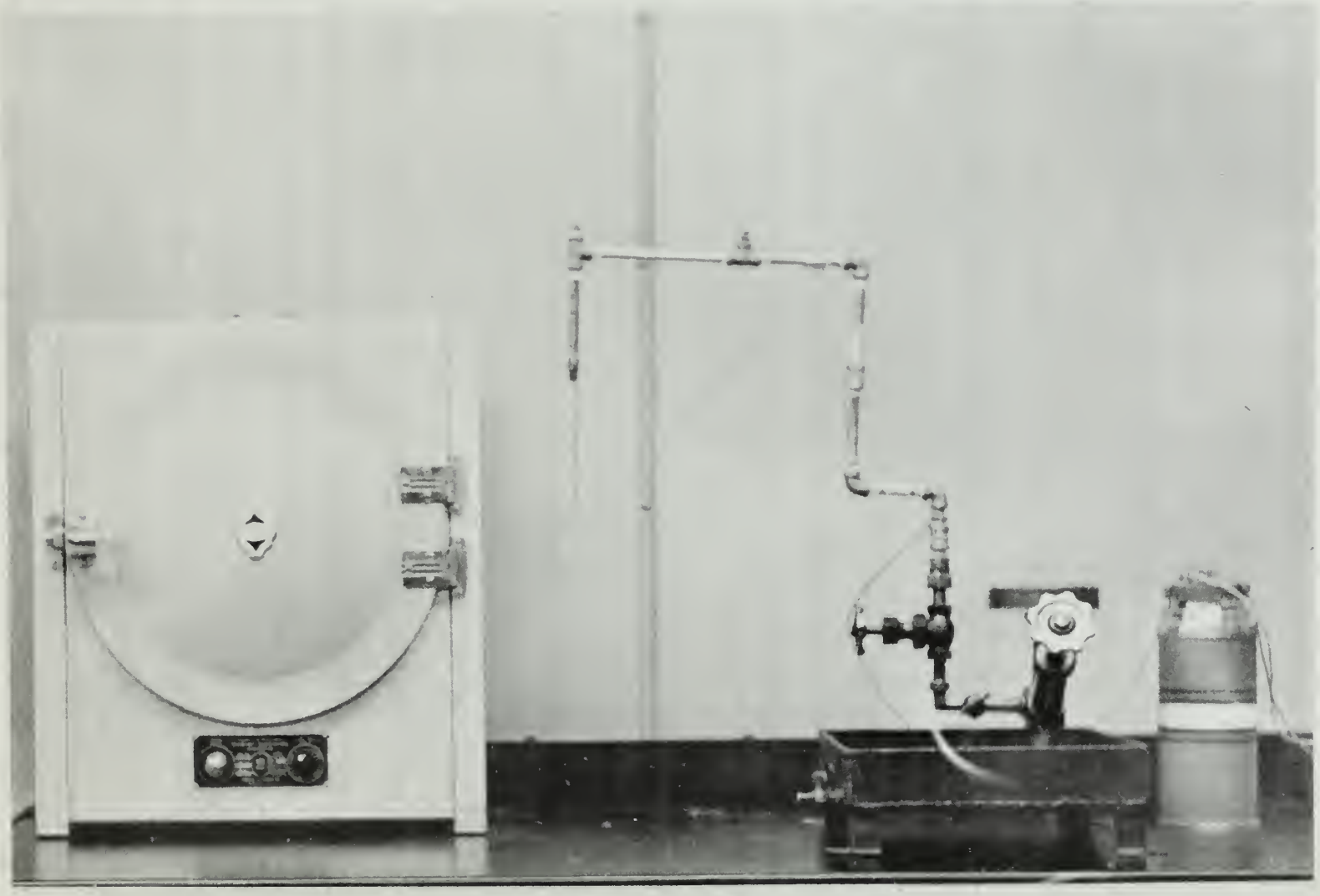

Figure 4. Oven And Loading Arrangement. The Thermocouple Junction Is At The End Of The Wire Protruding From The Loading Pipe.

leaking stopped. Expelling all the air before running a test was essential, since the total volume of oil in the loading system was small and the distance of travel of the loading screw was limited. With no air present in the system the load could be maintained with little movement of the loading piston. Otherwise, with air present, the end of the loading piston travel was reached before the cooling cycle was complete, and some hurried maneuvering was required in order to refill the oil reservoir while maintaining the required loading pressure on the model.

Section 6. Test Procedures

The model was filled with colorless mineral oil, then it was placed in the oil tank and connected to the loading piping. The system was filled with oil and initially pressurized to 20 psig to check for tightness. This load was removed and the vent plug was removed to allow for expansion of the oil during heating; thus, premature loading of a model was avoided. The desired maximum temperature for the cycle was set into the oven temperature control and heating commenced. After about 9 hours the equilibrium temperature, 280° F., was reached and the test load, 10 psig, was applied. About 45 minutes were allowed for the model response to reach equilibrium with the applied load, then the oven was turned off and allowed to cool. After the model had cooled, the load was removed and the model was ready for slicing and study.

The manner of slicing a model was determined by considering its geometry and symmetry. Each model consisted of three short cylinders having the same axis of symmetry and having junction planes normal to the axis. In cylindrical co-ordinates the three normal stresses acting upon an element are σ_r, the radial normal stress, σ_θ, the circumferential normal stress, and σ_z, the longitudinal normal stress. A thin

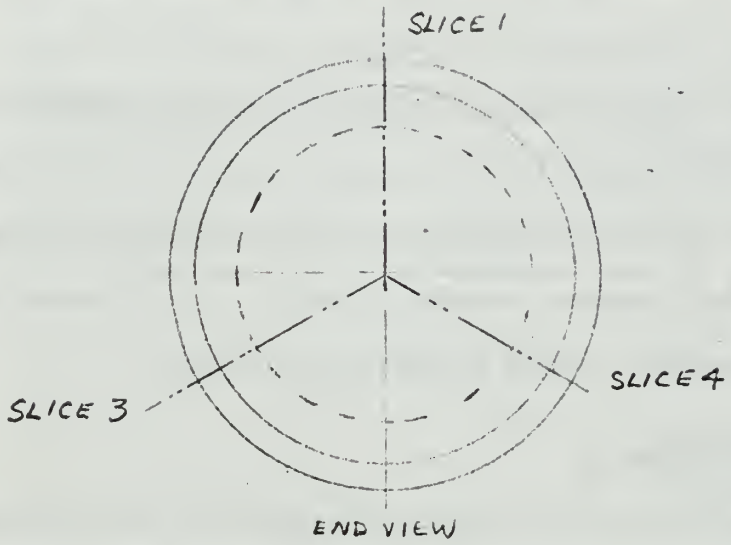

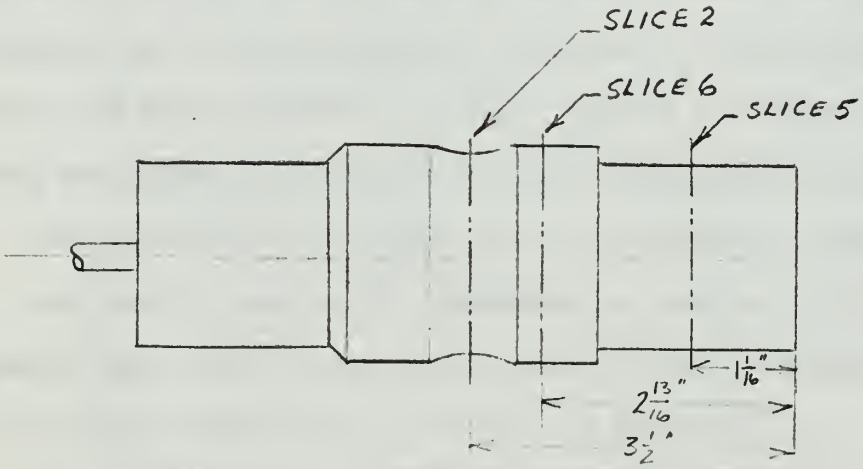

SLICE	THICKNESS (INCHES)
1	.192
2	.190
3	.189
4	.190
5	.142
6	.175

Figure 9. Slicing Plan For Model I.

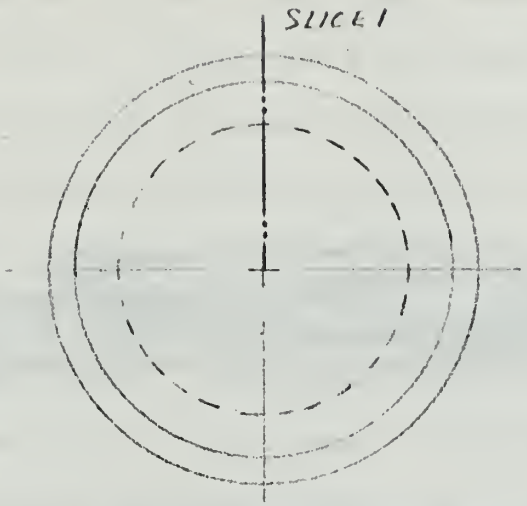

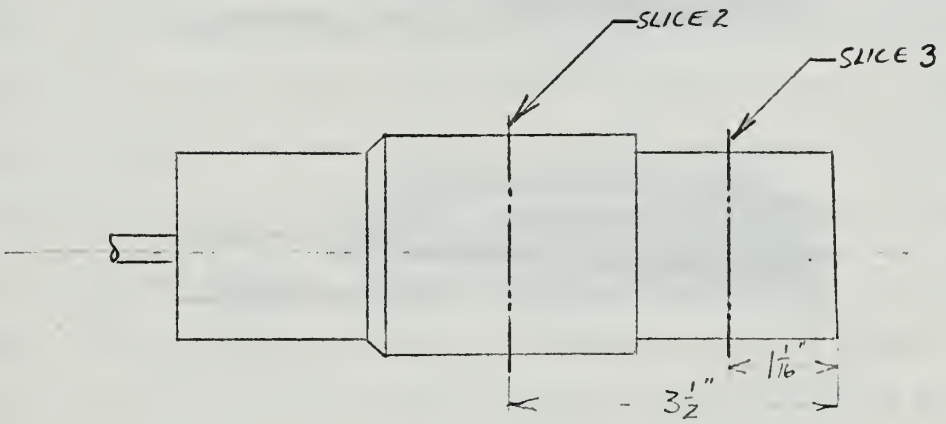

SLICE	THICKNESS (INCHES)
1	.200
2	.226
3	.202

Figure 10. Slicing Plan For Model II.

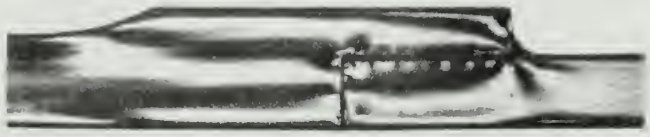

SLICE 1

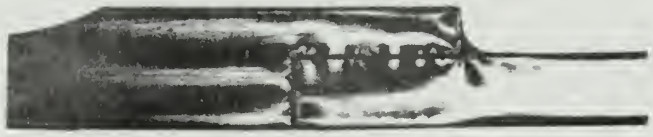

SLICE 3

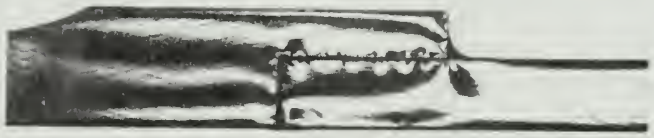

SLICE 4

Figure 1. Slice 1. Comparison of Slices Taken at 120 Degrees Apart. Slice Number Decreases as Response.

slice taken in a plane containing the axis of a cylinder contains only two principal stresses; at points away from a discontinuity these coincide with σ_z and σ_r . A slice taken in a plane normal to the axis also contains two principal stresses; these coincide with σ_θ and σ_r . Slices taken in a manner to coincide with the plane determined by two principal stresses may be analyzed in the same manner as two dimensional models, a far simpler process than is required for a more general three-dimensional stress analysis. The slicing plans,therefore, called for longitudinal slices and ring slices, each of which would contain a pair of principal stresses as described above.

The slicing plans for the models are shown in Figures 9 and 10. Model I had three longitudinal slices removed at 120 degree intervals as shown in the upper diagram of Figure 9 (slices 1, 3 and 4). These were made very nearly the same thickness so that inspection of the fringe patterns afforded an easy check for symmetry of response of the model to the applied loading. Figure 11 shows the comparison of these patterns. Model I also had three ring slices removed as shown in Figure 9. Model II was sliced in similar fashion as shown in Figure 10, but only one longitudinal slice and two ring slices were required.

Slicing was accomplished by using a sharp hand hacksaw with a blade having 32 teeth per inch. Slow careful sawing created only slight disturbances to the frozen fringe pattern. This distortion was automatically removed during subsequent finishing operations. Because of the small size of the slices, finishing was easily accomplished by hand sanding, using a succession of grit sizes, ending with worn 220 grit aluminum oxide paper. Saw marks were removed, coarse scratches eliminated, and

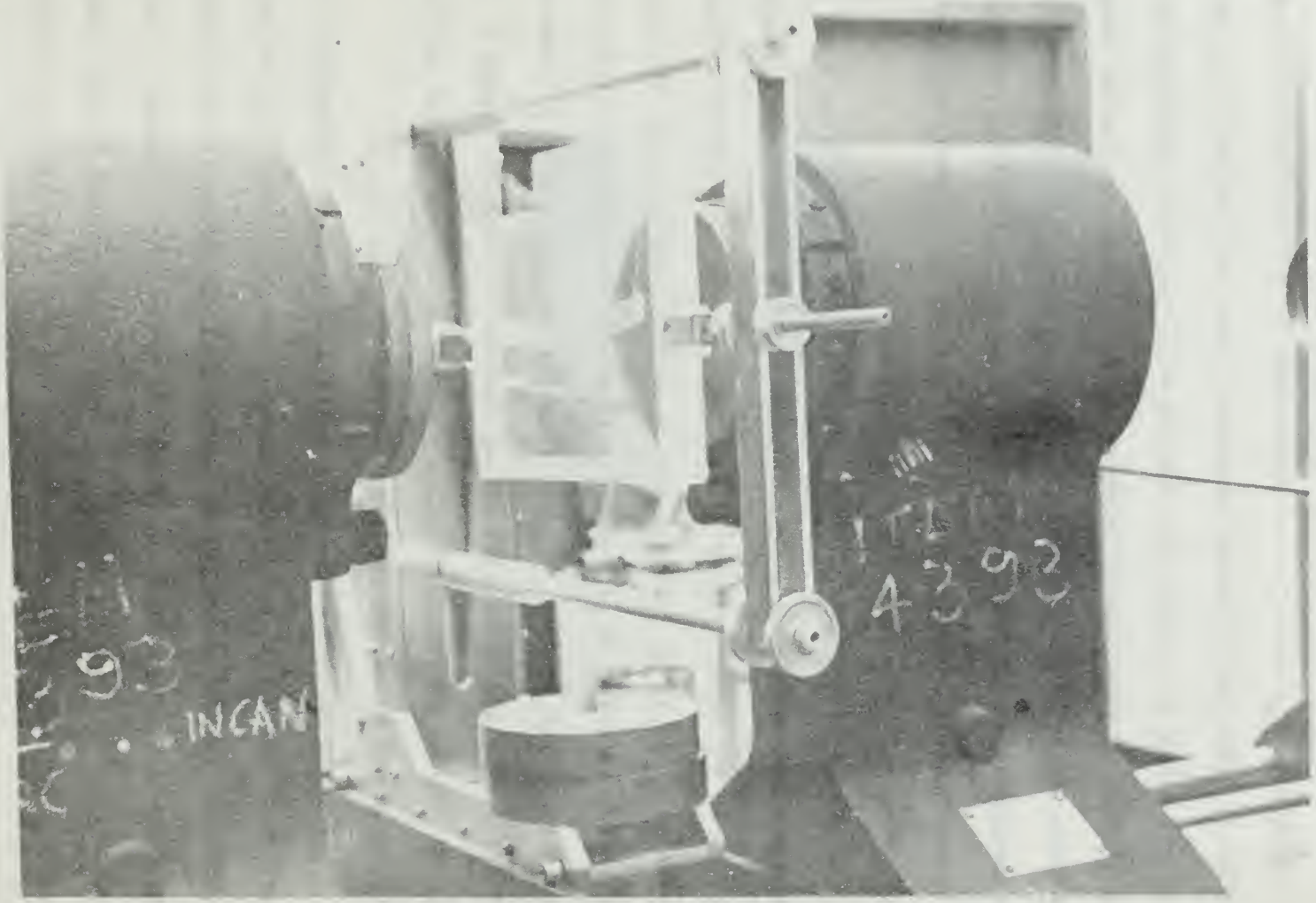
93
INCAN
A 393

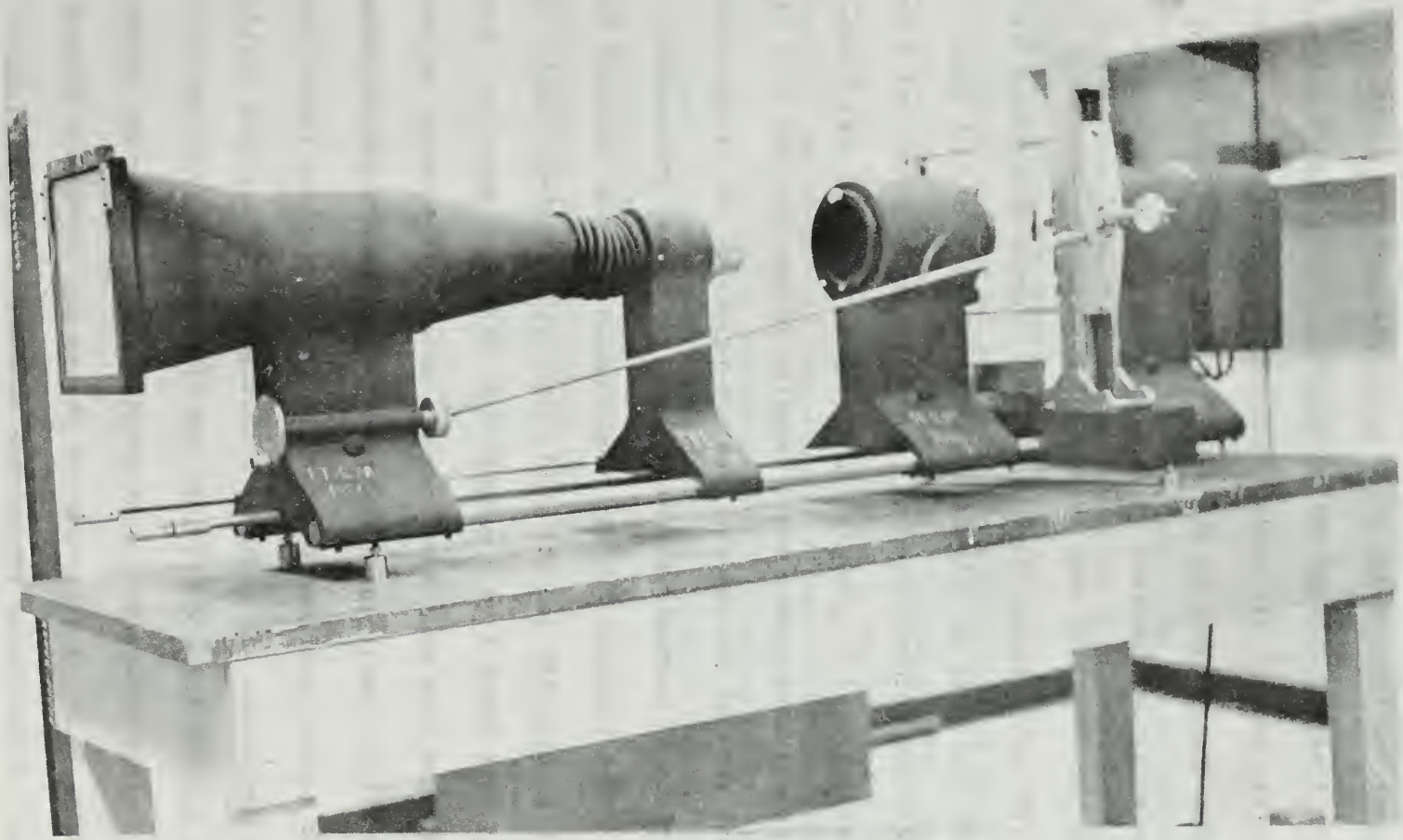

Figure 13. The Chavan Polariscope.

the slice thickness was adjusted until it was constant within .001 inch as measured with a micrometer caliper. Polishing was not required since an immersion tank having glass sides was used for containing the slices in the field of view of the polariscope. Preliminary tests showed that colorless mineral oil having an index of refraction of 1.4775 provided a close enough match to the epoxy so that photographs of the fringe patterns of slices immersed in this oil would be satisfactory. Figure 12 shows the immersion tank being used with the polariscope.

The polariscope, Figure 13, is a Chapman condensing type having a 5 inch field and an integral camera with an 8x10 inch back. Two light sources are interchangeable: one white light source and a mercury vapor source filtered to provide monochromatic light of 5461 Å wavelength. The camera arrangement makes negative images that are 2.07 times the actual size of the object. Contact prints of the fringe patterns were therefore of convenient size without additional enlargement.

Kodak Contrast Process panchromatic film was selected because of its high contrast and its good sensitivity to green light. Exposure times were about 1 to 2 seconds with wide open aperture. Fringe photography was done with open aperture because it provided an evenly illuminated field. Small apertures tended to produce a partial image of the light source superimposed upon the fringe pattern; this effect produced poor negatives. In general, both light field and dark field photographs were made of the model slices and calibration specimens.

Fringe orders were most conveniently found by the method described by Dally. [2] A wedge was cut across any convenient portion of the slice. A zero order fringe then appeared on the thin end of the wedge. This method was particularly applicable to the ring slices, where all

fringes were of high order. For the longitudinal slices, a free exterior corner provided a zero order starting point. A third method was to employ a stress frozen calibration beam as a compensator. This last method was found to be a useful supplement to the other two.

Section 7. Results of Tests

The objective of the investigation was to study the stress distributions for the two geometries in order to determine what differences existed as a result of the variations in geometry.

The simple body-of-revolution geometry allowed correlation with the Lame' solution for elastic stresses in thick-walled cylinders with internal pressure loading. The derivation of this solution is available from many texts; for example, see Dally. [2] The results of this solution are equations for σ_r and σ_θ , the radial and circumferential principal stresses, respectively. Figure 14 shows the diagram for the solution and indicates the meaning of the symbols employed.

The circumferential principal stress is:

$$\sigma_\theta = p_i \left(\frac{a^2}{b^2-a^2}\right)\left(1 + \frac{b^2}{r^2}\right) \qquad 7.1$$

The radial principal stress is:

$$\sigma_r = p_i \left(\frac{a^2}{b^2-a^2}\right)\left(1 - \frac{b^2}{r^2}\right) \qquad 7.2$$

where p_i = internal loading pressure, psig

a = inside radius

b = outside radius

r = radius (variable)

Equations 7.1 and 7.2 may be combined to yield a stress difference equation:

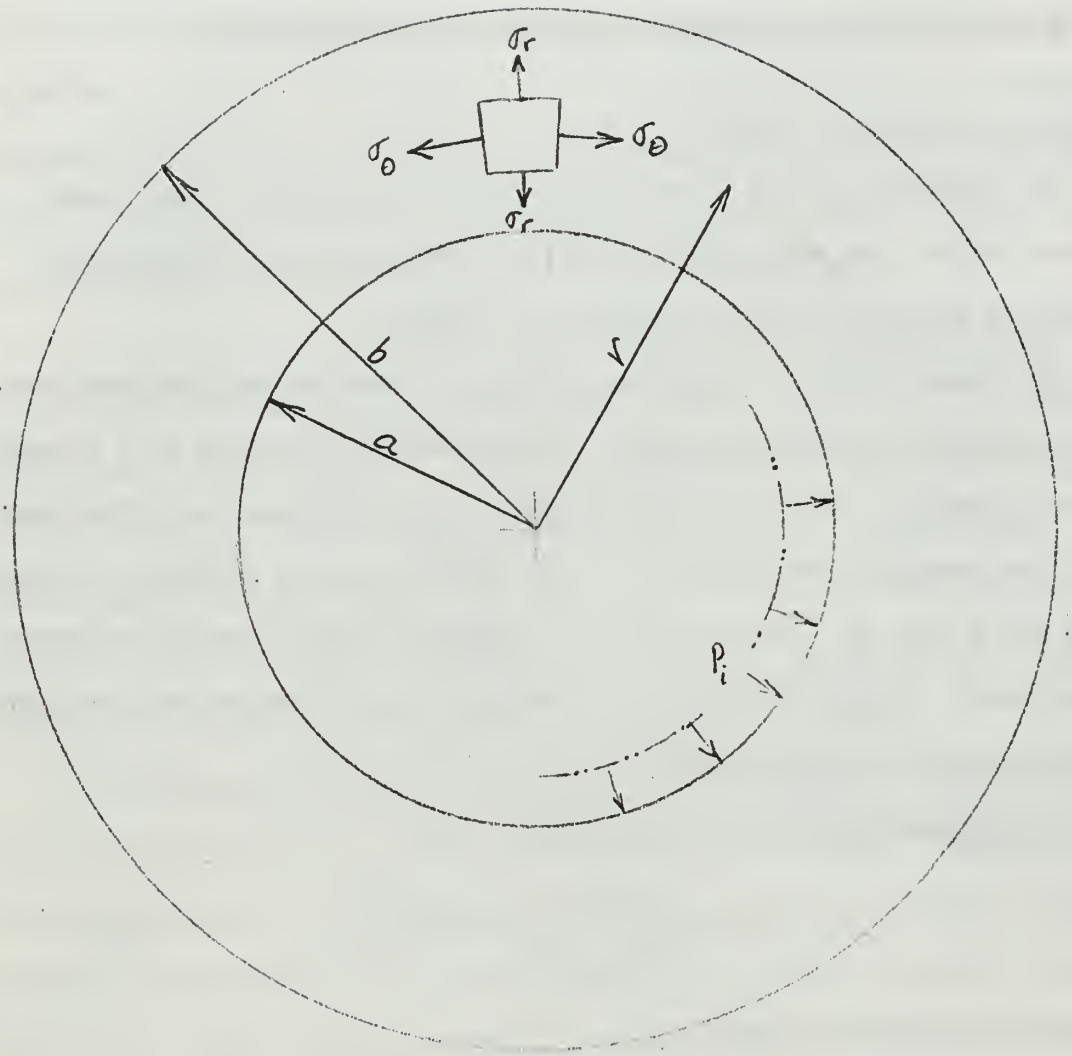

Figure 14. Diagram for The Lame' Solution For Principal Stresses In A Thick Walled Cylinder.

$$\sigma_\theta - \sigma_r = \frac{2p_i}{r^2}\left(\frac{a^2b^2}{b^2-a^2}\right) \qquad 7.3$$

Note that the photoelastic equation for a ring slice takes the form

$$\sigma_\theta - \sigma_r = \frac{Nf}{t} \qquad 7.4$$

where N = fringe order

f = material fringe value for stress, lb/in/fringe

t = slice thickness, in.

Now the experimental values for the stress difference could be compared with the theoretical values in order to check the reliability of the test results. The results of this comparison for the ring slices from Model I are shown in Figures 15, 16, and 17. The experimental points agree rather well with the predictions of the theory.

It should be noted that equations 7.3 and 7.4 may be combined and rearranged:

$$Nr^2 = \frac{t}{f}\left(\frac{2p_i a^2 b^2}{b^2-a^2}\right) \qquad 7.5$$

This relation may be used as a quick check on the consistency of a fringe photograph of ring slices, for the right hand side is a constant for a given slice.

Unfortunately, no such simple result was available to use for checking the longitudinal stress, σ_z , or the longitudinal stress difference, $\sigma_z - \sigma_r$. As mentioned in Section 2, simple cylindrical shell theory was not applicable because a third normal stress, σ_r , was present in addition to the two membrane stresses, σ_z and σ_θ . This radial stress was not negligibly small; in fact it frequently had a magnitude comparable

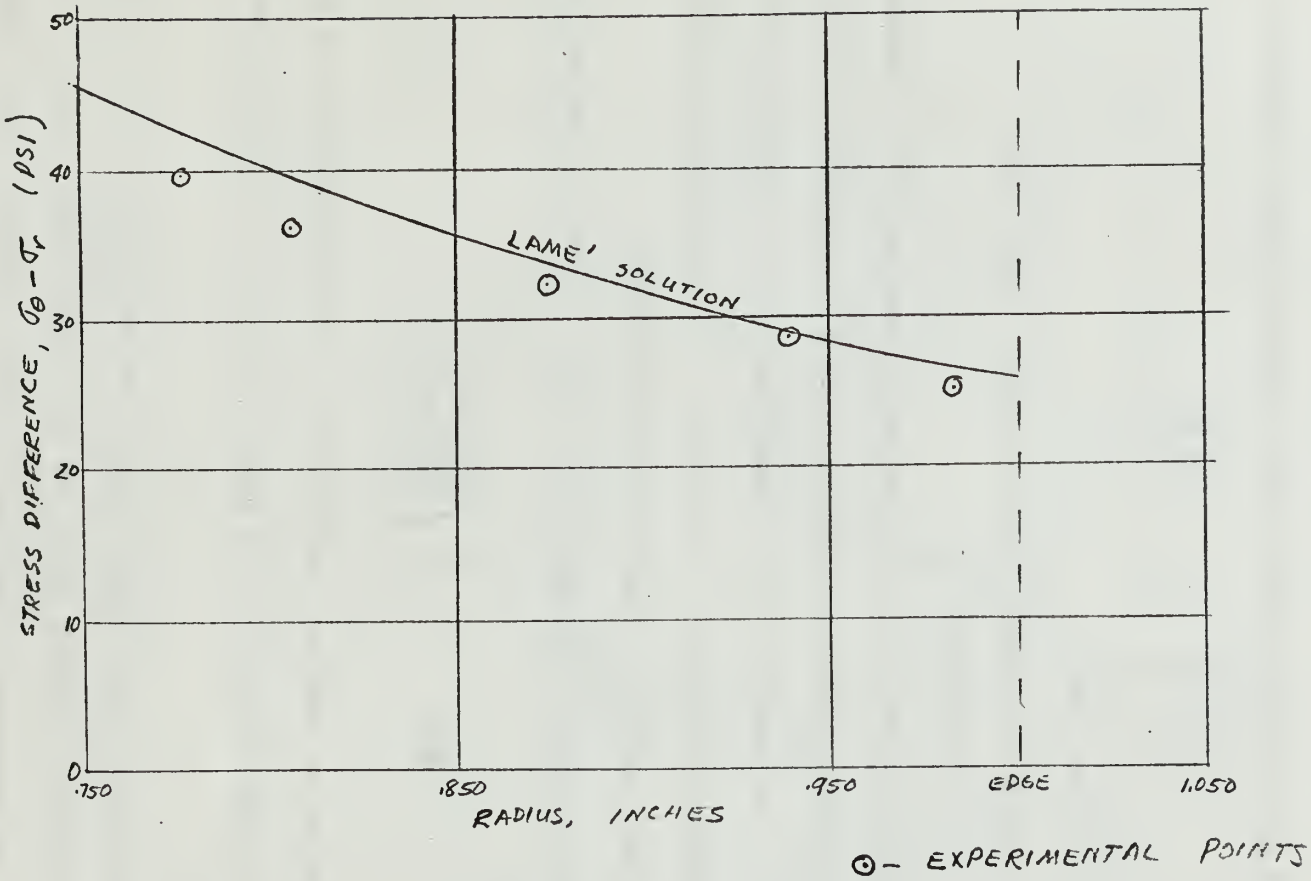

Figure 15. Model I, Slice 2. Comparison of Experimental and Theoretical Values of $\sigma_\theta - \sigma_r$.

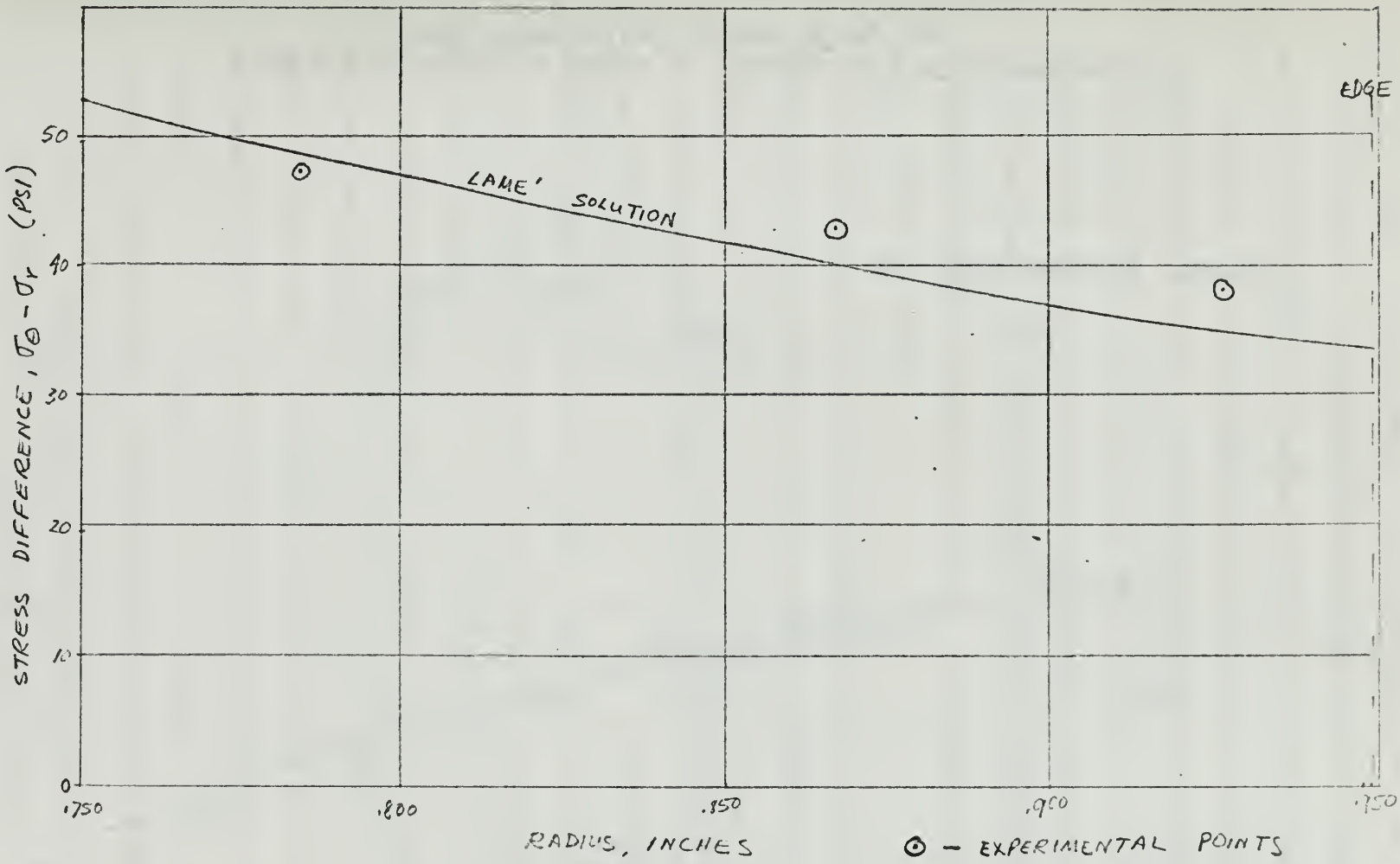

Figure 16. Model I, Slice 5. Comparison of Experimental and Theoretical Values of $\sigma_\theta - \sigma_r$.

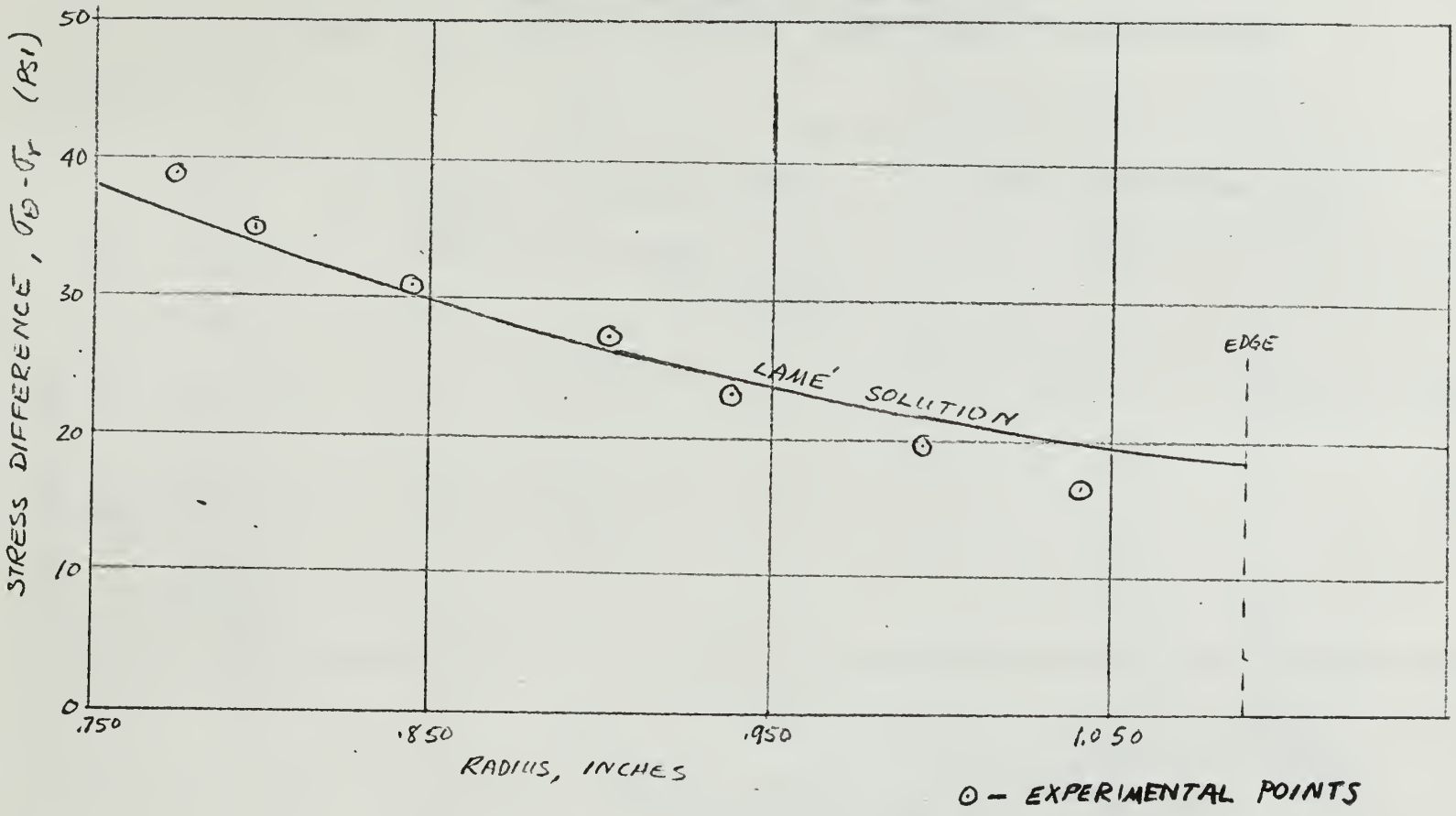

Figure 17. Model I, Slice 6. Comparison of Experimental and Theoretical Values of $\sigma_\theta - \sigma_r$.

to that of σ_z . Another factor causing difficulty was the presence of an edge moment at the junction of the smaller, 1.900 in. diameter cylinder and the larger, 2.200 in. diameter cylinder. This moment was the result of the change in the mean diameter of the cylinders at the plane of junction. Another effect resulted from the differing magnitudes of the radial and circumferential strains in each of the two cylinders at points just away from the junction plane. Compatibility requires that these strains be equal in the junction plane; this can be the case only with the existence of additional shearing forces and edge moments within the cylinders at the discontinuity.

A solution could be devised to this complicated problem by using some finite element numerical analysis scheme programmed for a digital computer, but this method of analysis is beyond the scope of this paper.

The good agreement in Model I of the experimental values of the stress differences in the ring slices with those obtained from the Lame' solution suggested that the theoretical value of σ_r in each case could be used as a method of separating the stresses in the longitudinal slices at locations where σ_z and σ_r were the principal stresses. Determination of σ_z by itself would make it possible to obtain a static check. The procedure followed in this process was first to obtain a fringe order vs. radius curve. Multiplying the order by the slice fringe value furnished the value of the stress difference at each point. The Lame' solution curve for $-\sigma_r$ was plotted on the same axes. The difference in ordinates between the σ_z-σ_r curve and the $-\sigma_r$ curve was plotted as the curve for σ_z . This last result was then used to plot a curve of $\sigma_z r$ vs. r. The static check at a section required a summation of the normal stress over the area of the section, an integration of the form

$$P = 2\pi \int_a^b \sigma_z r \, dr \qquad 7.6$$

where $P = \pi a^2 p_i$ = the normal force at a section. The value of the integral in equation 7.6 was found graphically by applying Simpson's rule to find the area under the $\sigma_z r$ vs. r curve. This area was multiplied by 2π and the graph scale factor for the area units to yield the value of P. The appropriate graphs and the calculations for Model I may be found in Appendix II. For statics to be satisfied this value of P had to be identical to the opposing force, the result of the internal pressure acting on the inside cross sectional area of the cylinder. The result of this check for Model I is shown in the following table.

SECTION	STATIC CHECK LOAD, Lb.	APPLIED LOAD, Lb.	% DIFFERENCE
Pipe	18.3	17.3	+ 6
Coupling	16.3	17.3	- 6

The differences are considered acceptable for a static check.

The curves of σ_z vs. radius were useful for determining the behavior of the model, but with certain reservations. The stress distribution generally followed what was expected considering that shell bending was superimposed upon the normal Lamé stresses. For example, in the curve for the zone of slice 5 (the pipe) in Figure 25, σ_z is seen to be largest in the outer fibers and smallest inside. This follows, for the shell bending moment at this section must have produced tensile stresses in the outer fibers and compressive stresses in the inner fibers, all superimposed on a constant σ_z of about 16.3 psi. Similarly, in the coupling section at slice 6 the σ_z curve shown in Figure 28 shows some bending effects in the opposite sense, for the largest values are near the inner surface of the coupling. In these curves the photoelastically

determined values of σ_z were low at the boundaries. These values are probably erroneous for two reasons: first, it is possible that the "time-edge effect" superimposed local compressive stresses upon the already existing tensile system; or second, that the low indicated fringe order near a boundary may have resulted from the variation in slice thickness at the boundary, a natural consequence of the fact that the surfaces at the boundaries are portions of cylindrical surfaces rather than planes. If these edge effects are ignored, the other indicated values of σ_z appear to be believable.

The longitudinal slices, numbers 1, 3, and 4, showed in their fringe patterns that there was some sort of stress concentration taking place at the discontinuity of the junction, but the slice geometry and characteristics of the cement produced rather broad shadows which effectively obliterated the fine pattern which may have existed at the junction of the cylinders. For this reason no stress concentration factor was obtained for this discontinuity.

The slight difference in the ends of the coupling proved to be insignificant. It did not alter the stress distribution except to make a somewhat smoother transition between the small cylinder and the large cylinder at the end having the 45 degree bevel.

The analysis of Model II was conducted in similar fashion, but the results were erratic. Figures 35 and 36 in Appendix III show the comparison of the photoelastic stress difference and the theoretical Lame' curve for the coupling and pipe ring slices. For the coupling slice the experimental values are all low by what appears to be a nearly constant amount. The single experimental point for the pipe slice fell remarkably close to the theoretical curve, making the two sets of results

mutually inconsistent. Whatever affected slice 2 apparently did not affect slice 3. Another check on the experimental results was to attempt to satisfy statics as was done for Model I. The ring slice results did not completely justify the assumption that the Lamé values for σ_r could be used to separate the principal stresses, but a static check was made using this assumption as an approximation. The stress distribution for the section at the center of the coupling is shown in Figure 38, and the σ_z r vs. r curve with its accompanying force calculations are shown in Figure 39 and following in Appendix III. The calculated force here was only 11.6 lb., 33% lower than the applied load of 17.3 lb. This tended to confirm that the results of Model II were too much in error to be quantitatively useful.

Although good numerical results were not obtainable from the test of Model II, some inferences may be gathered from Model I about the influence of the circumferential groove on the stress distribution. The fringe pattern of slice 1 from Model I (Figure 19) shows the distortion of the pattern at the groove that corresponds to the increase in level of the stress intensity at the narrowing section. It appears that extending the fringe pattern on either side of the groove would yield a pattern corresponding to the coupling with no groove. Alternatively, the results of the analysis for the zone of slice 6 could be used to represent the plain coupling. Figure 40 shows the variation of σ_z with radius for the section taken at the groove. It shows an approximate mean stress of 15 psi, while the mean stress of the undiminished section is about 9 psi. The ratio of these stresses is about 1.7. The corresponding inverse ratio of the cross section areas is about 1.4. This shows very roughly that the stress level in the section at the groove is affected largely by the decrease

in section area.

Section 8. Suggestions for Further Investigation

A cemented model such as was used to represent brazed joints is not very good for studying the effects of discontinuities. A one-piece model with cast or cemented ends would be better because the effects would be much clearer. Cement lines, shadows and attendant air bubbles would all be eliminated. The geometry at corners and fillets would be easier to control because of the absence of cement in these important areas.

Determination of boundary stresses depends upon freedom from the time-edge effect. In the tests described, even very rapid handling of the models and slices was not adequate to avoid some interference from this effect.

BIBLIOGRAPHY

1. Burke, Robert E. Photoelastic Study of Pressure Vessel Stresses. Unpub. M. S. Thesis, U. S. Naval Postgraduate School, 1955.

2. Dally, J. W. and Riley, W. F. Experimental Stress Analysis. McGraw-Hill, 1965.

3. Hetenyi, M. Ed. Handbook of Experimental Stress Analysis. Wiley, 1950.

4. Pih, H. "Three Dimensional Photoelastic Investigation of Circular Cylinders with Spherical Cavities in Axial Loading." Experimental Mechanics, v. 5, March, 1965: 88-95.

5. Timoshenko, S. and Woinowsky-Krieger, S. Theory of Plates and Shells, 2nd Ed. McGraw-Hill, 1959.

APPENDIX I

MATERIAL AND MODEL DATA

Technical Data for Hysol 4290

Typical Properties

Critical temperature		270° F
Tensile strength	@ 77° F	12000 psi
	@ 270° F	210 psi
Modulus of elasticity	@ 77° F	480000 psi
	@ 270° F	2190 psi
Poisson's ratio		.500
Fringe value	@ 77° F	57 lb/in-fringe
	@ 270° F	1.35 lb/in-fringe
Annealing temperature		280° - 300° F

***

Model I Actual Dimensions

Inside diameter	1.500 in.
Pipe outside diameter	1.898 in.
Coupling outside diameter	2.177 in

***

Model II Actual Dimensions

Inside diameter	1.500 in.
Pipe outside diameter	1.891 in.
Coupling outside diameter	2.177 in.

Calibration Beam Moment Calculations

Applied Load:

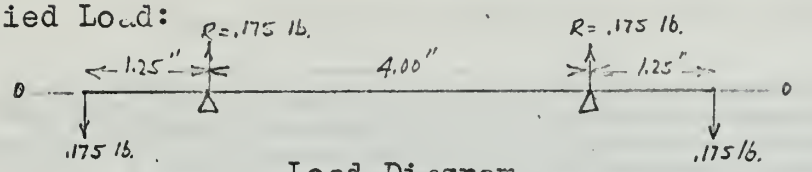

Load Diagram

Shear Diagram

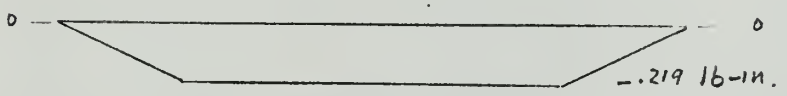

Moment Diagram

Gravity Load:

Density of epoxy	.053 lb/in^3
Density of oil	.030 lb/in^3
Apparent weight of beam	.021 lb
Load	.0029 lb/in

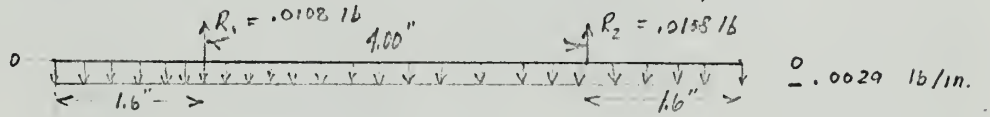

Load Diagram

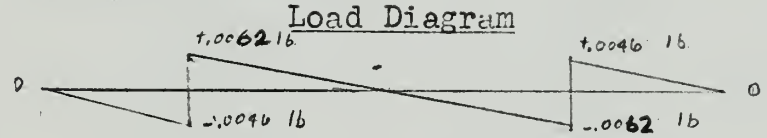

Shear Diagram

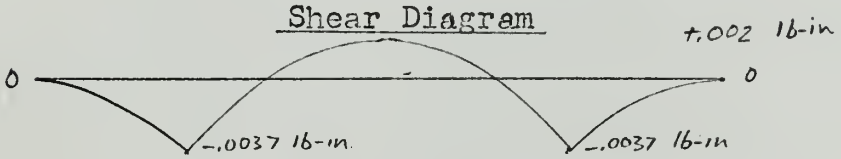

Moment Diagram

(Maximum moment in the center span is less than 1% of the applied moment.)

Figure 18. Typical Calibration Beam Fringe Pattern.

TABLE OF CALIBRATION VALUES OF f

SPECIMEN	f, lb/in/fringe
2	1.32
3	1.35
4	1.34
5	1.39
Average	1.37

APPENDIX II

MODEL I FRINGE PHOTOGRAPHS AND CALCULATIONS

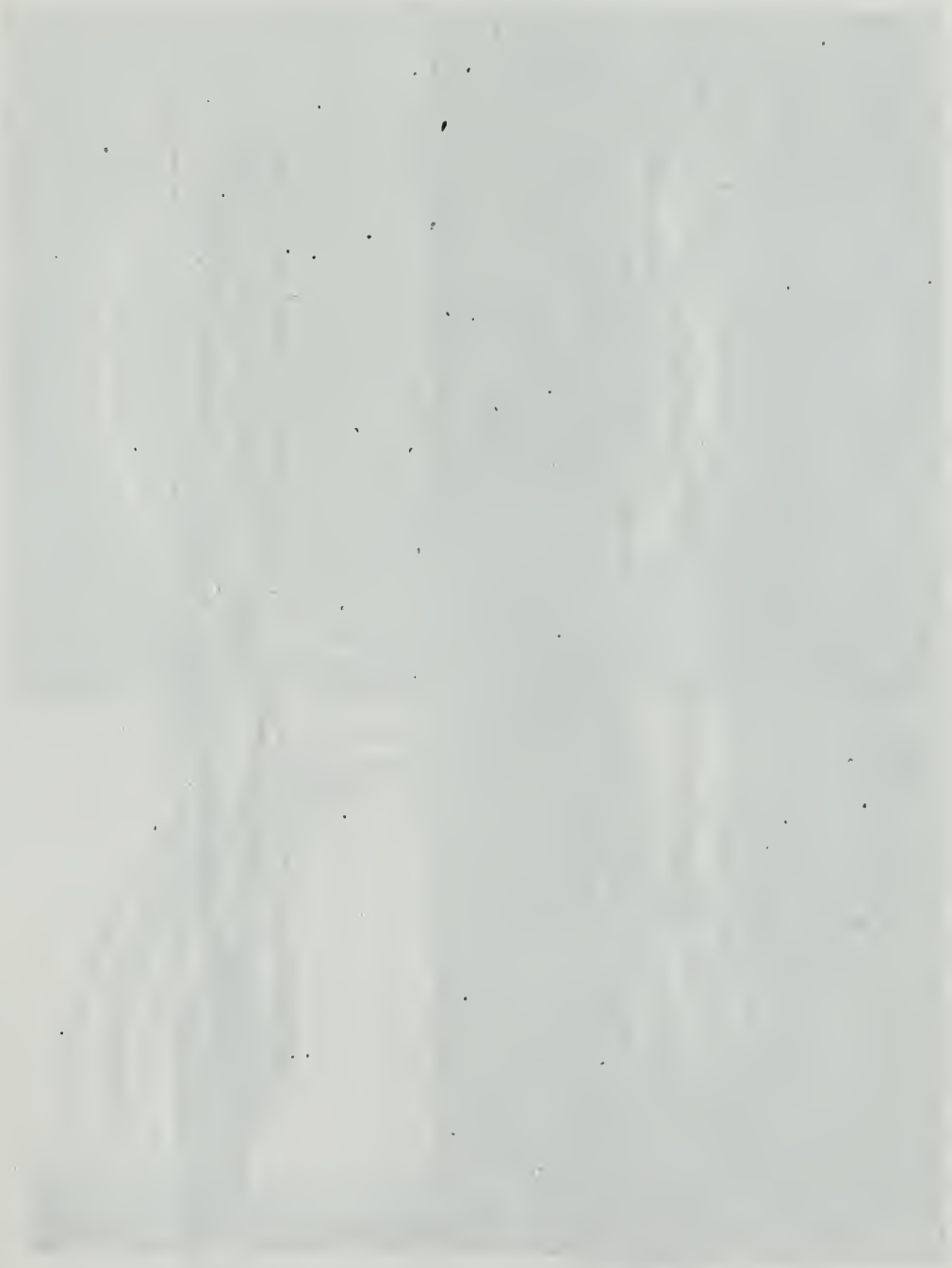

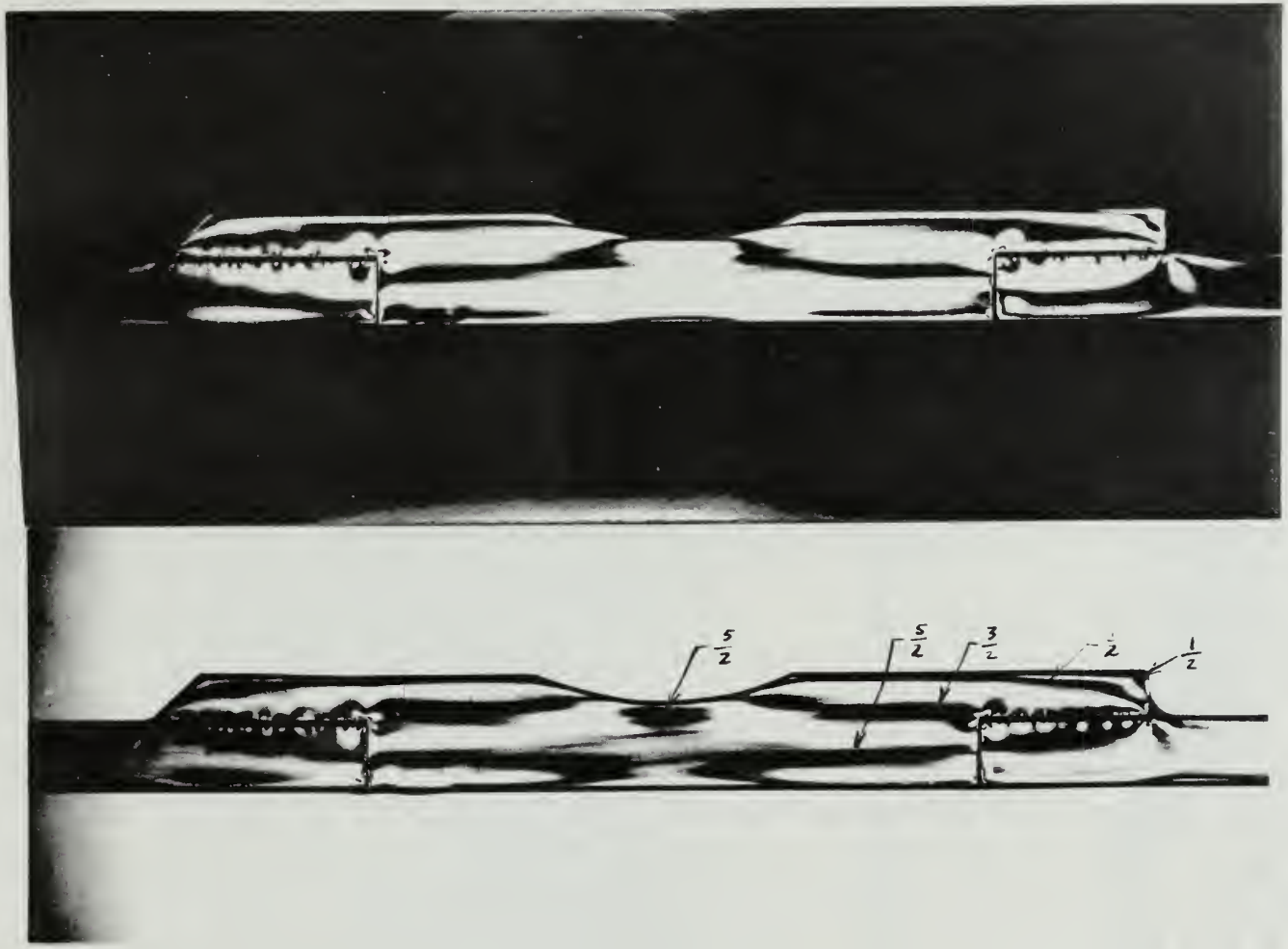

Figure 1. Model I, Slice 1. Fringe Patterns for Dark and Light Field.

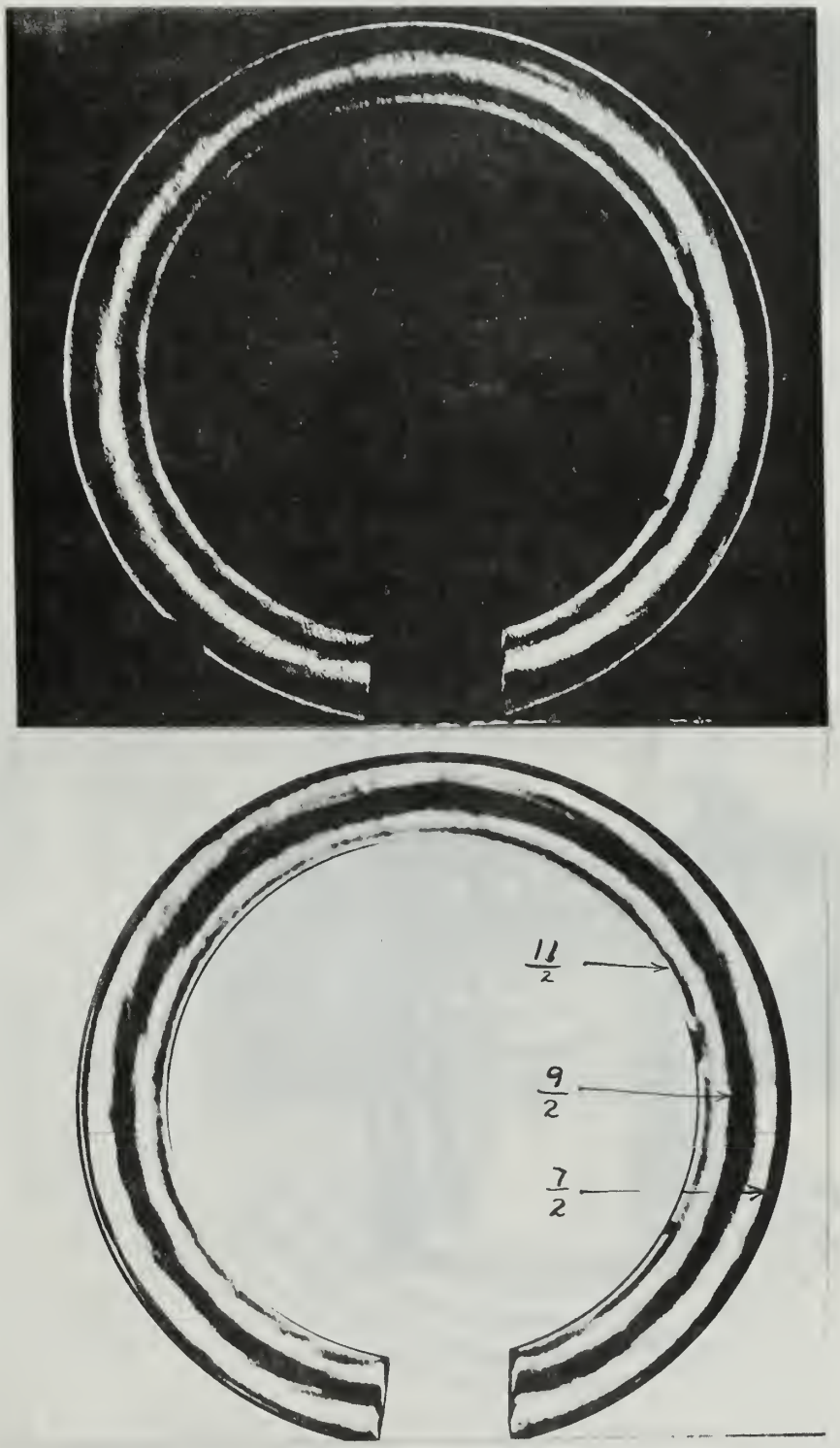

Figure 20. Model I, Slice 2. Fringe Patterns for Dark and Light Field.

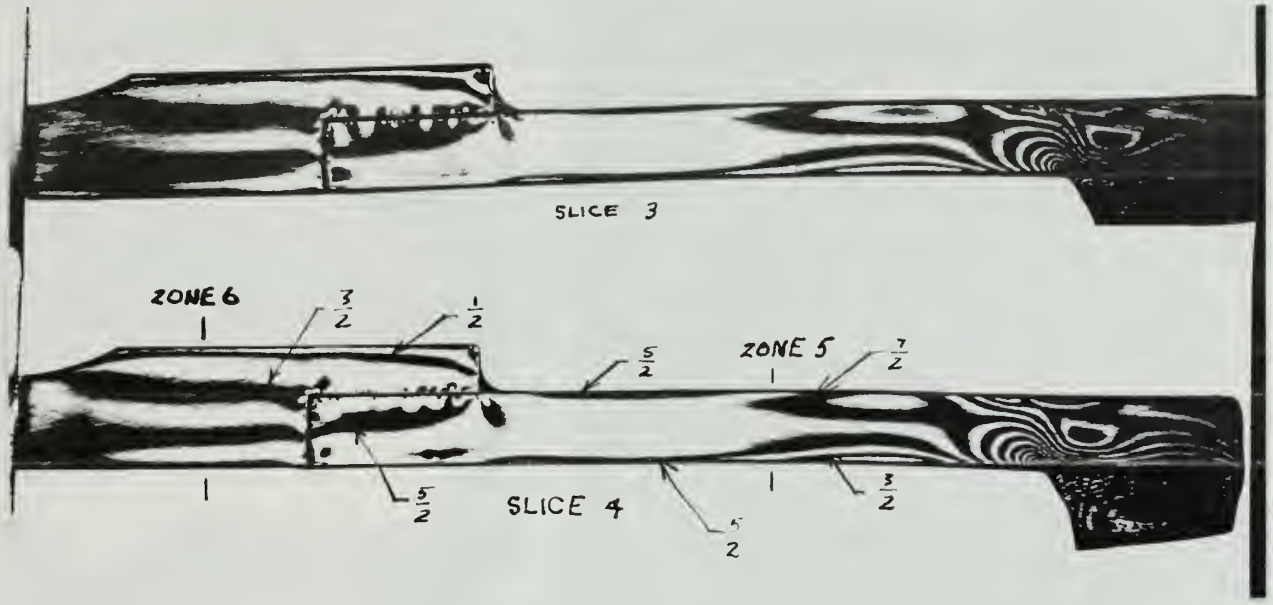

Figure 21. Model I, Slices 3 and 4. Fringe Patterns for Light Field.

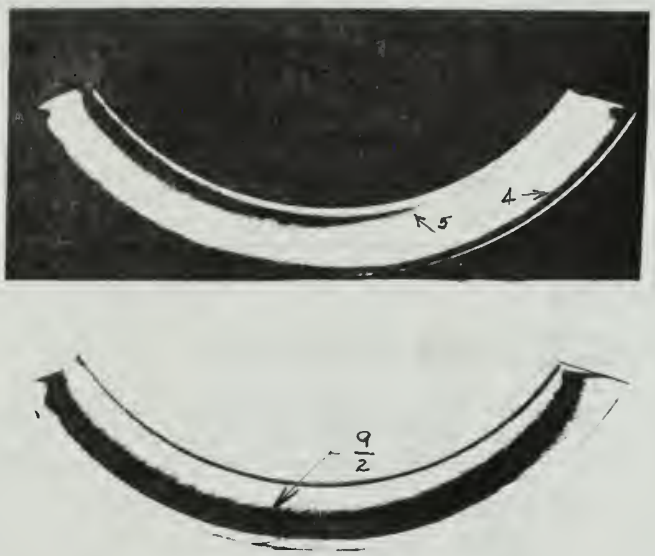

Figure 22. Model I, Slice 5. Fringe Patterns for Dark and Light Field.

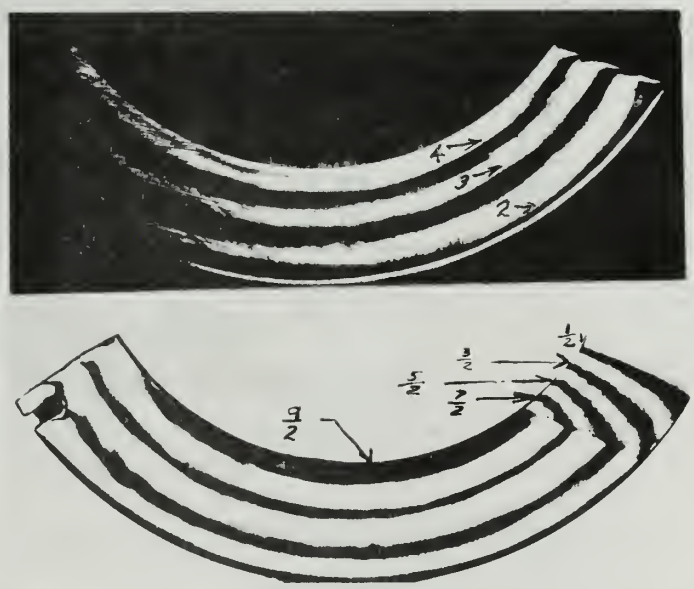

Figure 23. Model I, Slice 6. Fringe Patterns for Dark and Light Field.

MODEL I CALCULATIONS FROM PHOTOGRAPH DATA

Slice 2

$\frac{f}{t} = \frac{1.37}{.196} = 7.2$ psi/fringe

N	r, in.	$\sigma_\theta - \sigma_r$, psi	$\sigma_\theta - \sigma_r$ (Lamé), psi
3.5	.982	25.2	26.6
4	.938	28.8	29.2
4.5	.873	32.4	33.6
5	.806	36.0	39.5
5.5	.777	39.6	42.5

Slice 5

$\frac{f}{t} = \frac{1.37}{.142} = 9.62$ psi/fringe

N	r, in.	$\sigma_\theta - \sigma_r$, psi	$\sigma_\theta - \sigma_r$ (Lamé), psi
4	.926	38.4	34.8
4.5	.866	43.3	40.0
5	.784	48.1	48.6

Slice 6

$\frac{f}{t} = \frac{1.37}{.175} = 7.8$ psi/fringe

N	r, in.	$\sigma_\theta - \sigma_r$, psi	$\sigma_\theta - \sigma_r$ (Lamé), psi
2	1.04	15.6	19.9
2.5	.992	19.5	21.9
3	.938	23.4	24.4
3.5	.902	27.3	26.4
4	.844	31.2	30.5
4.5	.798	35.1	33.8
5	.775	39.0	35.8

MODEL I LONGITUDINAL STRESS CALCULATIONS
FROM PHOTOGRAPH DATA

Slice 4

$\frac{f}{t} = \frac{1.37}{.190} = 7.2$ psi/fringe

Zone 5

N	r, in.	$\sigma_z - \sigma_r$, psi	σ_r, psi	σ_z, psi	σ_{zr}, lb/in
2	.750	14.4	-10.0	4.4	3.3
2.5	.786	18.0	-7.6	10.4	8.2
3	.850	21.6	-4.0	17.6	14.9
3.5	.910	25.2	-1.4	23.8	21.6
3	.949	21.6	0	21.6	20.5

Zone 6

N	r, in.	$\sigma_z - \sigma_r$, psi	σ_r, psi	σ_z, psi	σ_{zr}, lb/in
2.5	.750	18.0	10.0	8.0	6.0
3	.788	21.6	8.2	13.4	10.5
2.5	.832	18.0	6.4	11.6	9.6
2	.890	14.4	4.5	9.9	8.8
1.5	.953	10.8	2.8	8.0	7.6
1	1.028	7.2	1.0	6.2	6.4
.5	1.064	3.6	0.4	3.2	3.4

Zone 2

N	r, in.	$\sigma_z - \sigma_r$, psi
2.5	.96	18
3	.77	21.6

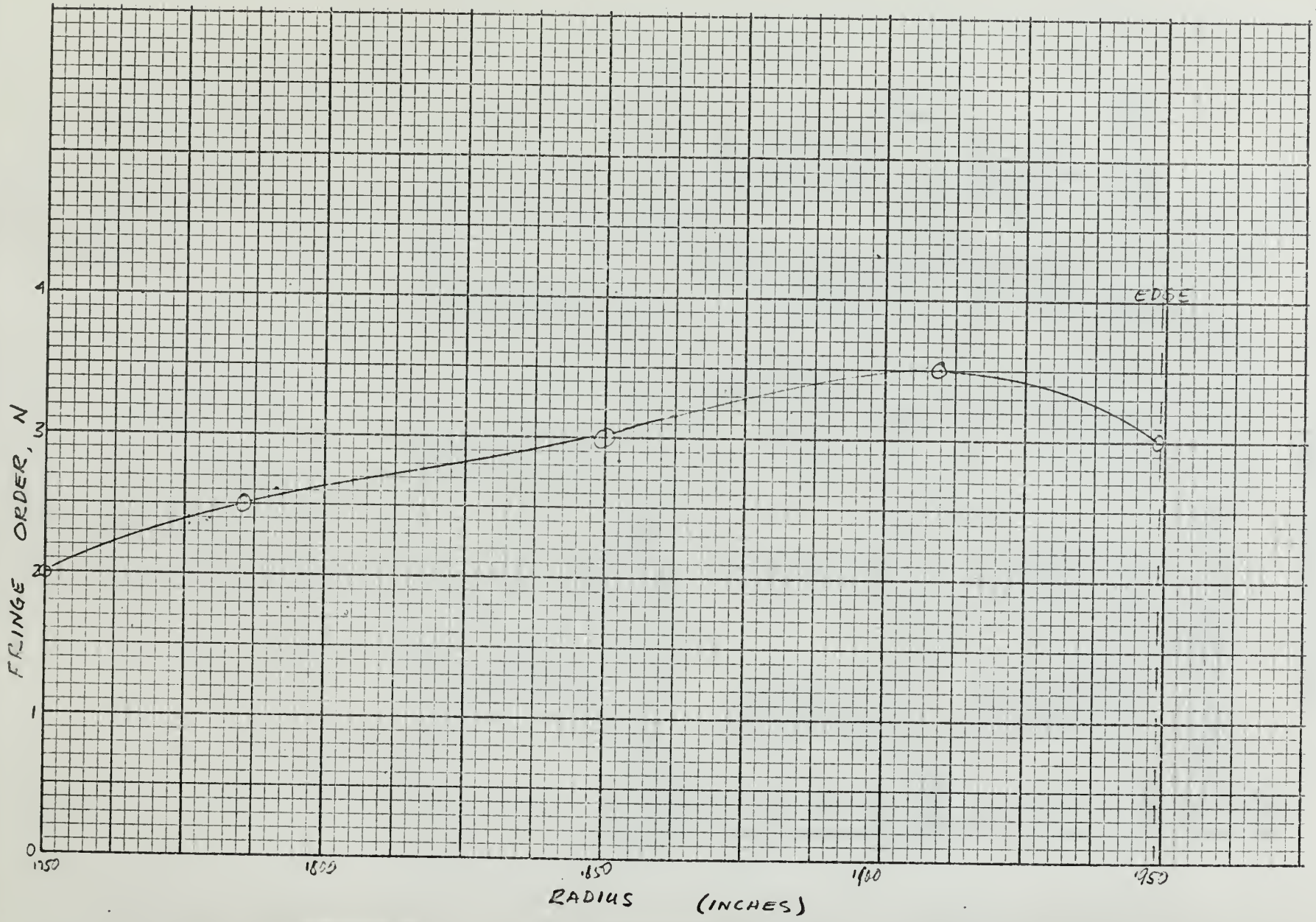

Figure 24. Model I, Slice 4. Fringe Order vs. Radius at Zone 5.

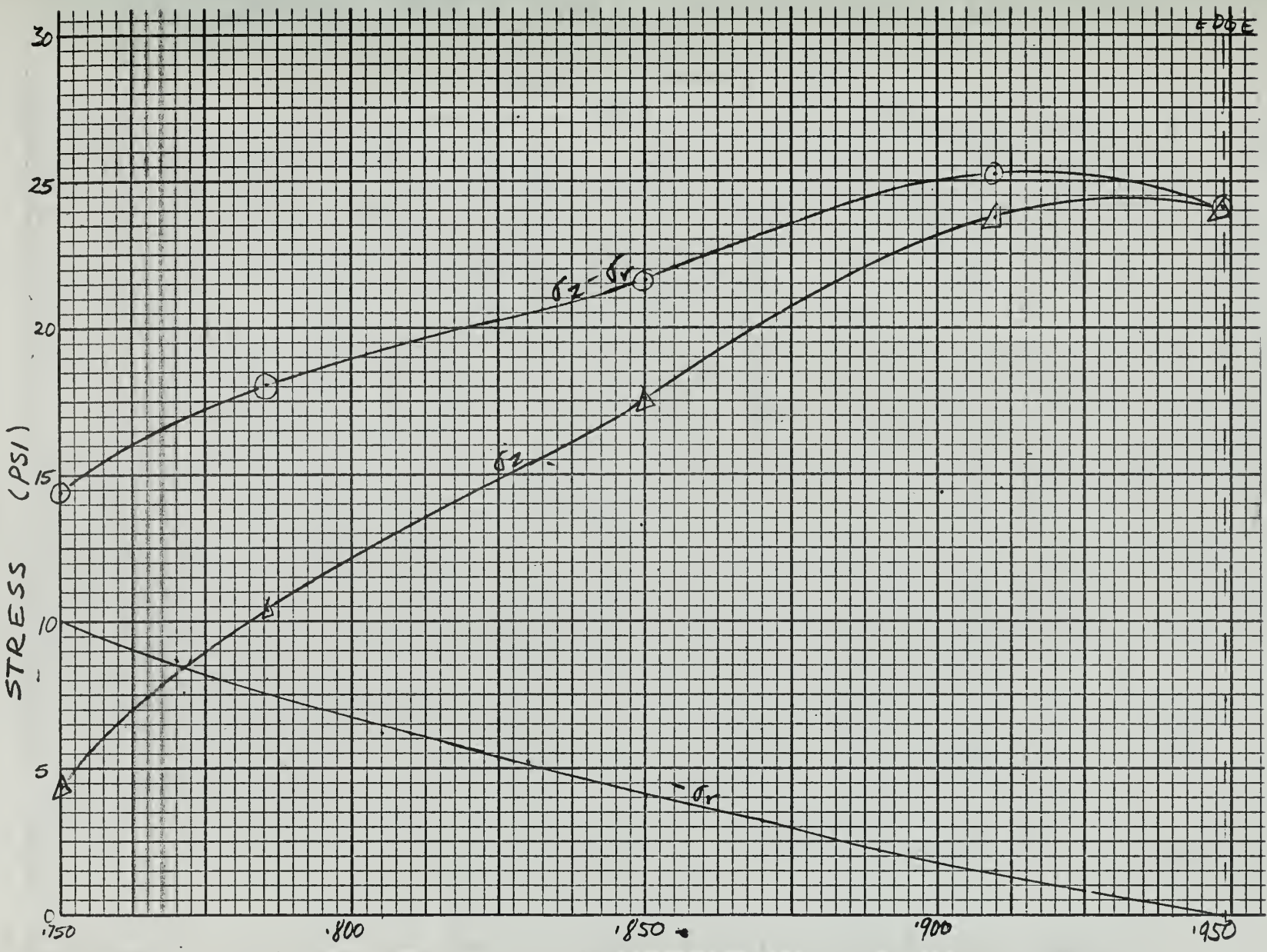

Figure 25. Model I, Slice 4. Stress Distribution at Zone 5.

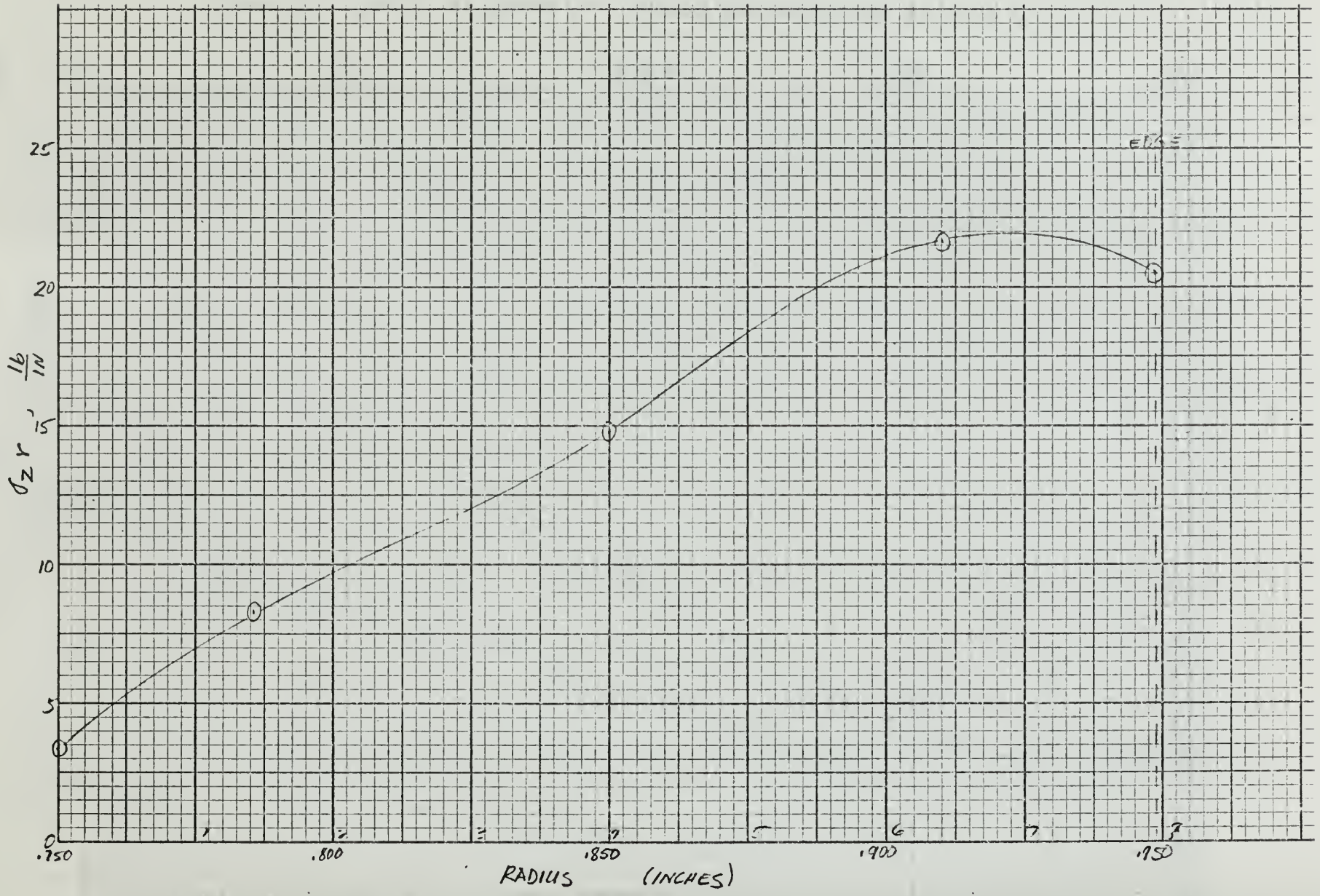

Figure 26. Model I, Slice 4. Curve for Graphical Force Summation at Zone 5.

MODEL I STATIC CHECKS

Zone 5 (See Figure 26.)

Simpson's rule was applied to the $\sigma_z r$ vs. r curve in order to find the value of $\int_a^b \sigma_z r\,dr$. The abscissa was divided into 8 segments of 1 inch on the graph, having a scale value of .025 inch. This yields an area too large by the amount of the excess included in the last segment; call this area A'. Then the required area is A = A' - .16 square inches.

$$A' = \frac{1}{3}\left[(.66+4.1)+4(1.4+2.4+3.7+4.4)+2(1.9+2.9+4.2)\right]$$

$$A' = 23.53 \text{ sq. in.}$$

$$A = 23.37 \text{ sq. in.}$$

Graph area value = .125 lb.

$$\therefore P=(2\pi)(23.37)(.125)=18.3 \text{ lb.}$$

Considering internal pressure loading on inside cross section: $P = p\pi a^2$

$$P=(10)(\pi)(.75)^2 = 17.3 \text{ lb.}$$

Per cent difference:

$$\frac{18.3-17.3}{17.3} \times 100 = +6\%$$

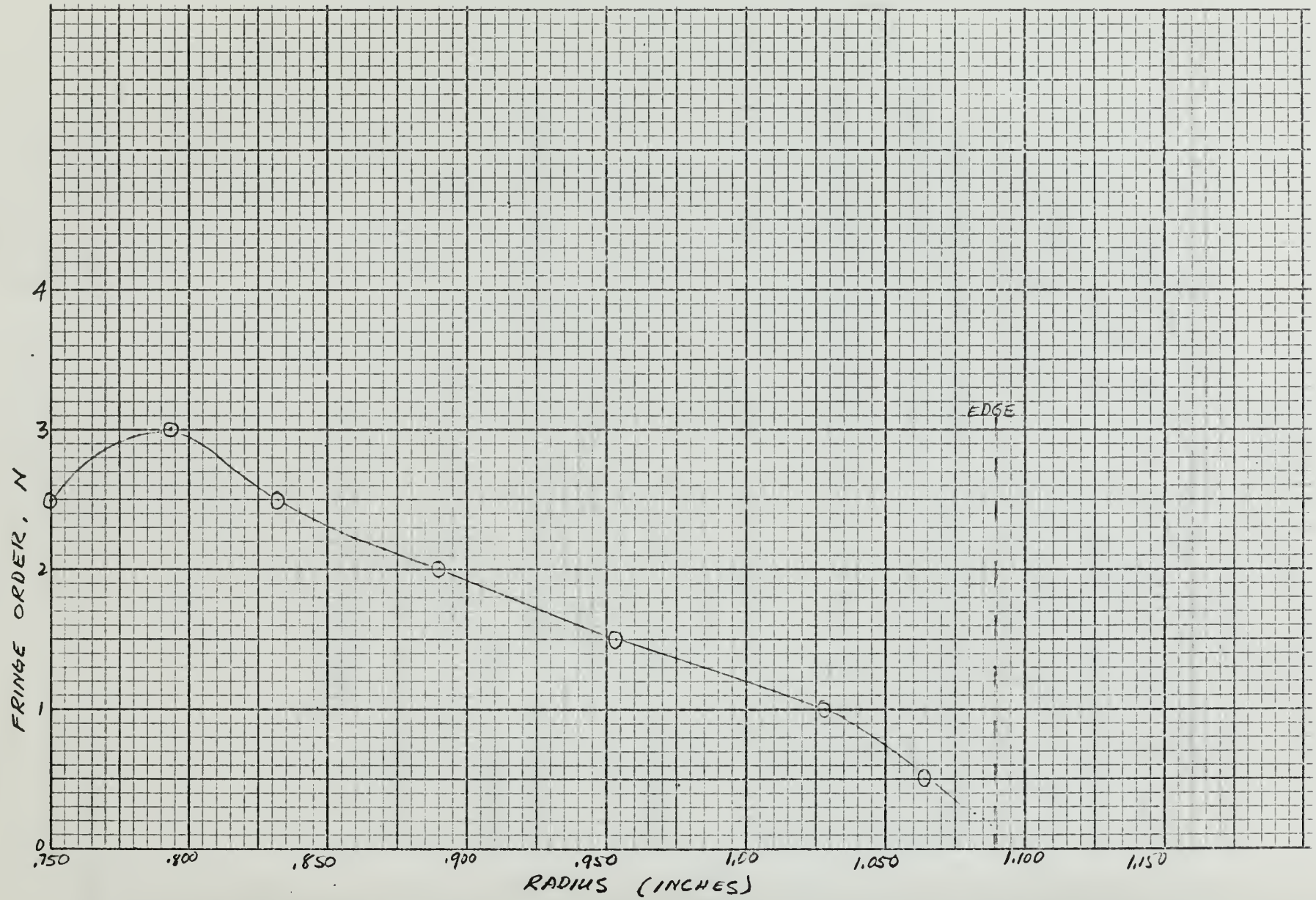

Figure 27. Model I, Slice 4. Fringe Order vs. Radius at Zone 6.

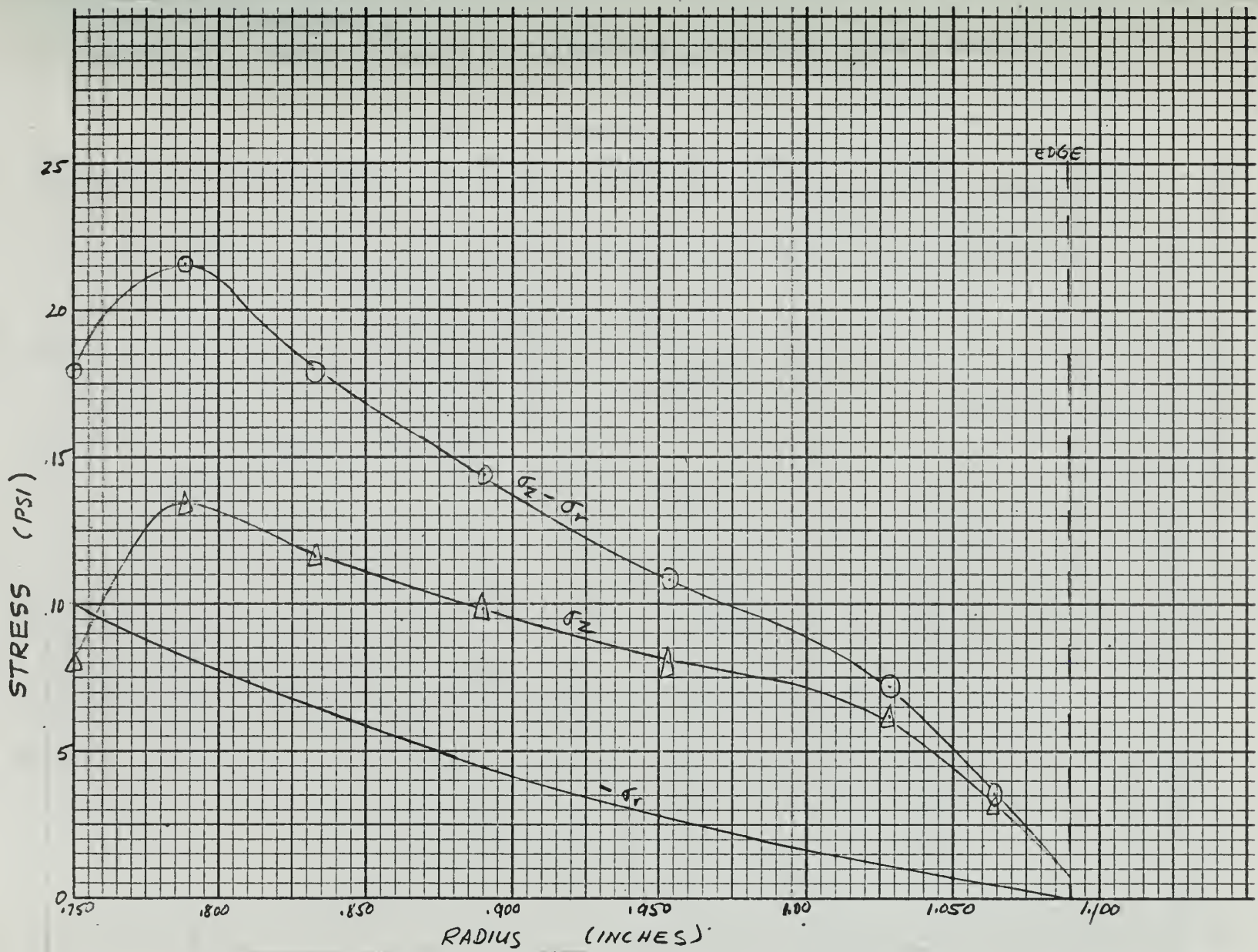

Figure 28. Model I, Slice 4. Stress Distribution at Zone 6.

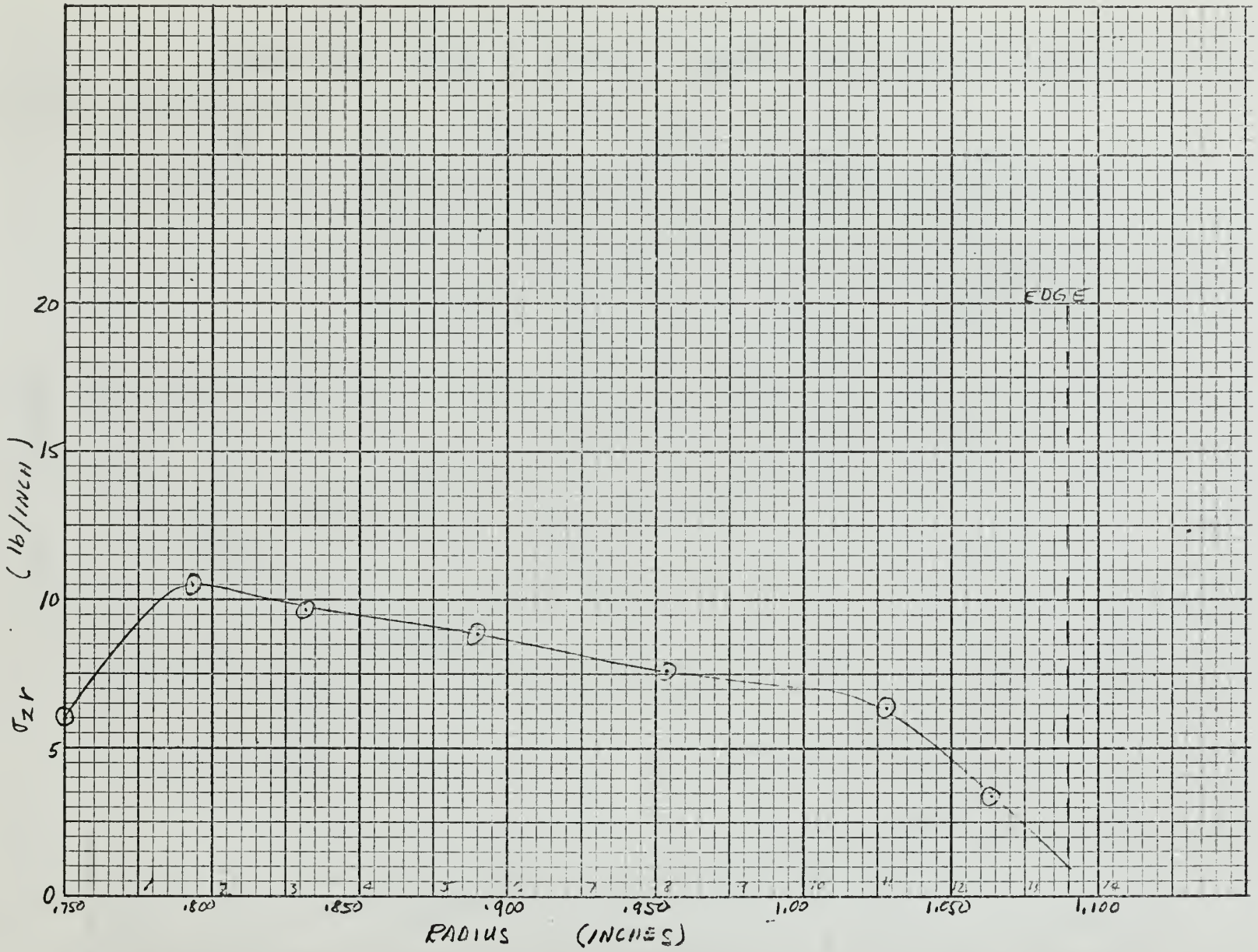

Figure 29. Model I, Slice 4. Curve for Graphical Force Summation at Zone 6.

MODEL I STATIC CHECKS

Zone 6 (See Figure 29.)

Simpson's rule was applied with the abscissa divided into 14 segments 1/2 inch long. The area unit used was a square 1/2 x 1/2 inch having a scale value of .0625 lb.

$A = A' - .08$ sq. units

$$A' = \frac{1}{3}\left[(2.4+.4)+4(3.7+3.0+3.6+3.3+2.9+2.6+1.0) + 2(4.2+3.8+3.5+3.0+2.8+1.8)\right]$$

$A' = 41.67$ sq. units

$A = 41.59$ sq. units

Graph area value = .0625 lb.

$$P = (41.59)(2\pi)(.0625) = 16.3 \text{ lb.}$$

Considering internal pressure loading on the inside cross section: $P = p_i \pi a^2$

$$P = (10)(\pi)(.75)^2 = 17.3 \text{ lb}$$

Per cent difference:

$$\frac{16.3 - 17.3}{17.3} \times 100 = -6\%$$

APPENDIX III

MODEL II FRINGE PHOTOGRAPHS AND CALCULATIONS

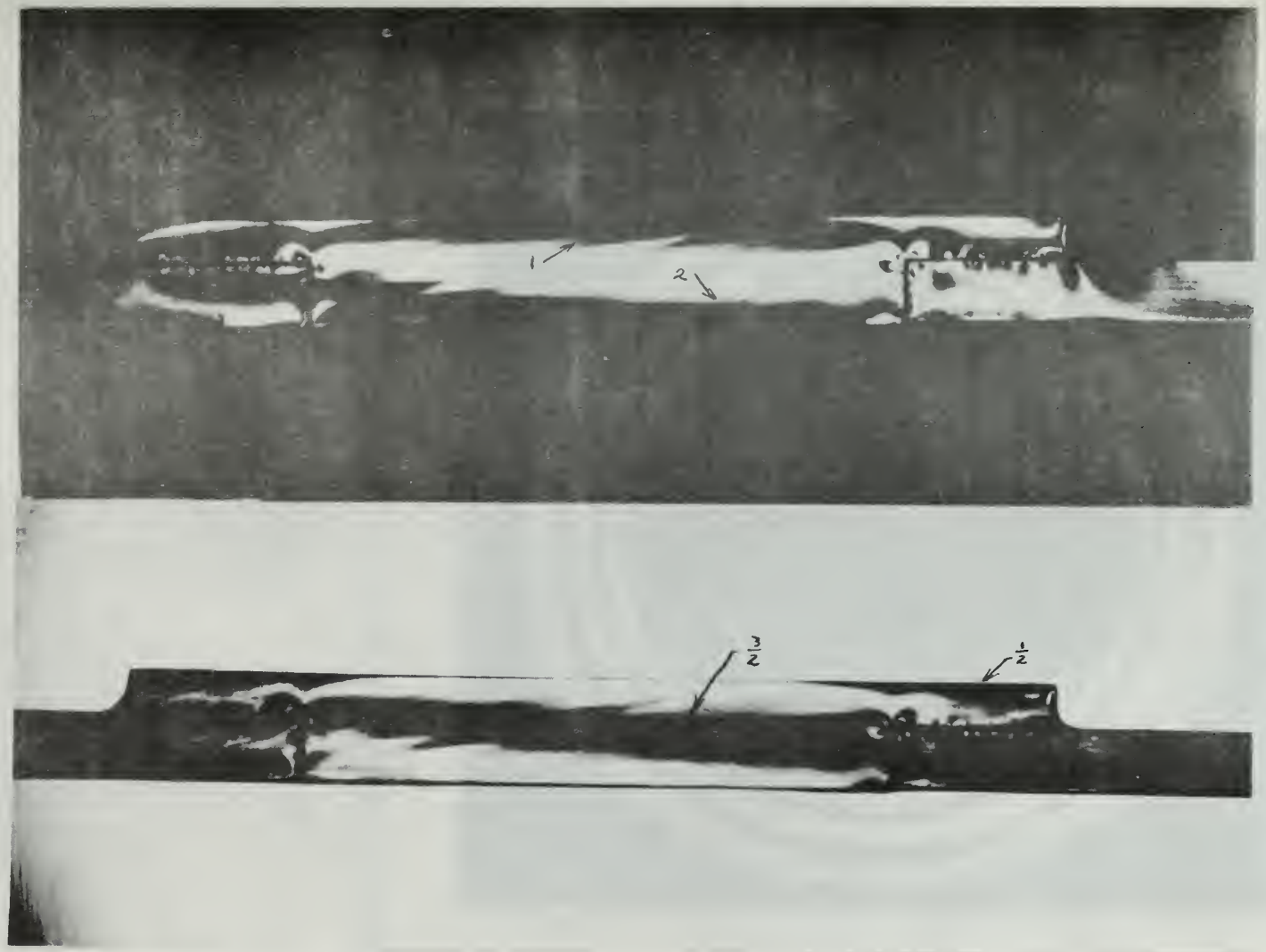

Figure 30. Model II, Slice 1. Fringe Patterns for Dark and Light Field.

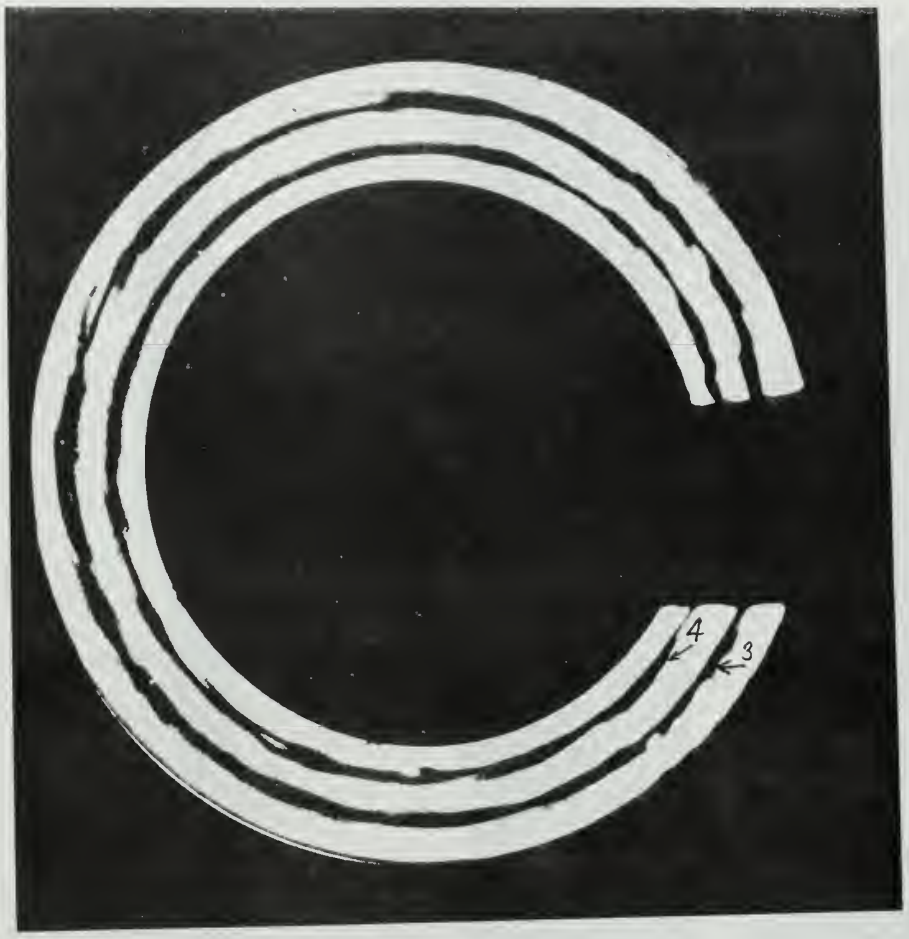

Figure 31. Model II, Slice 2. Fringe Pattern for Dark Field.

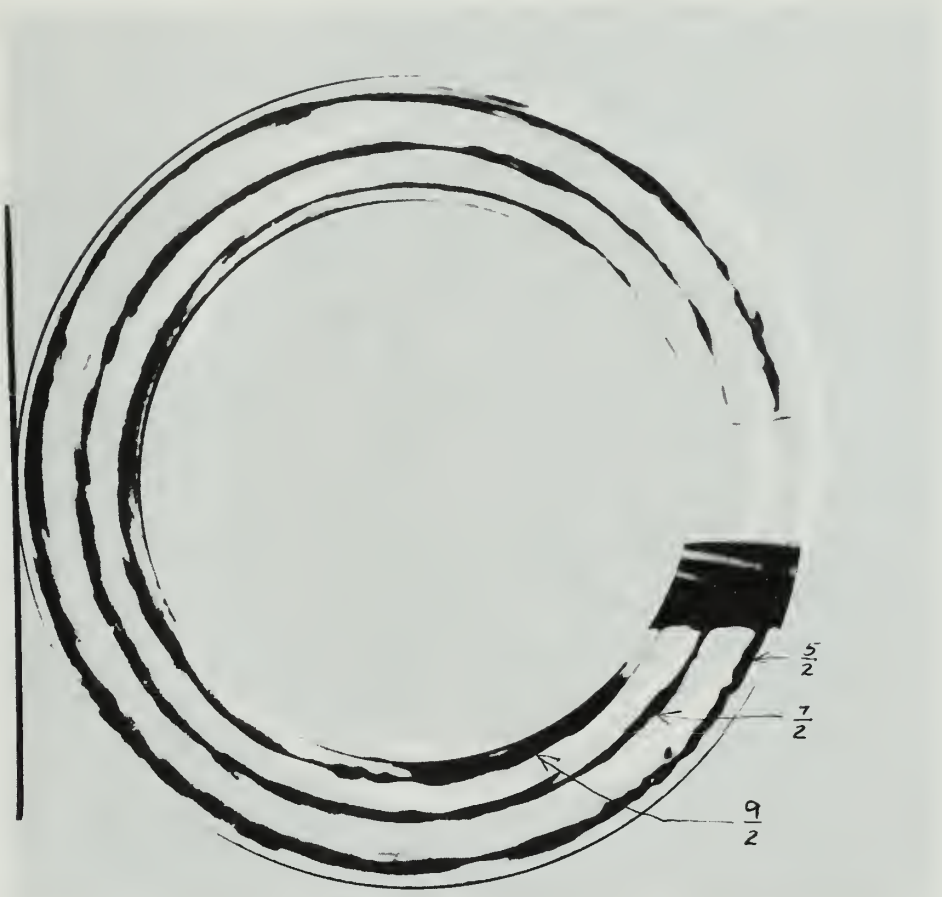
5/2
7/2
9/2

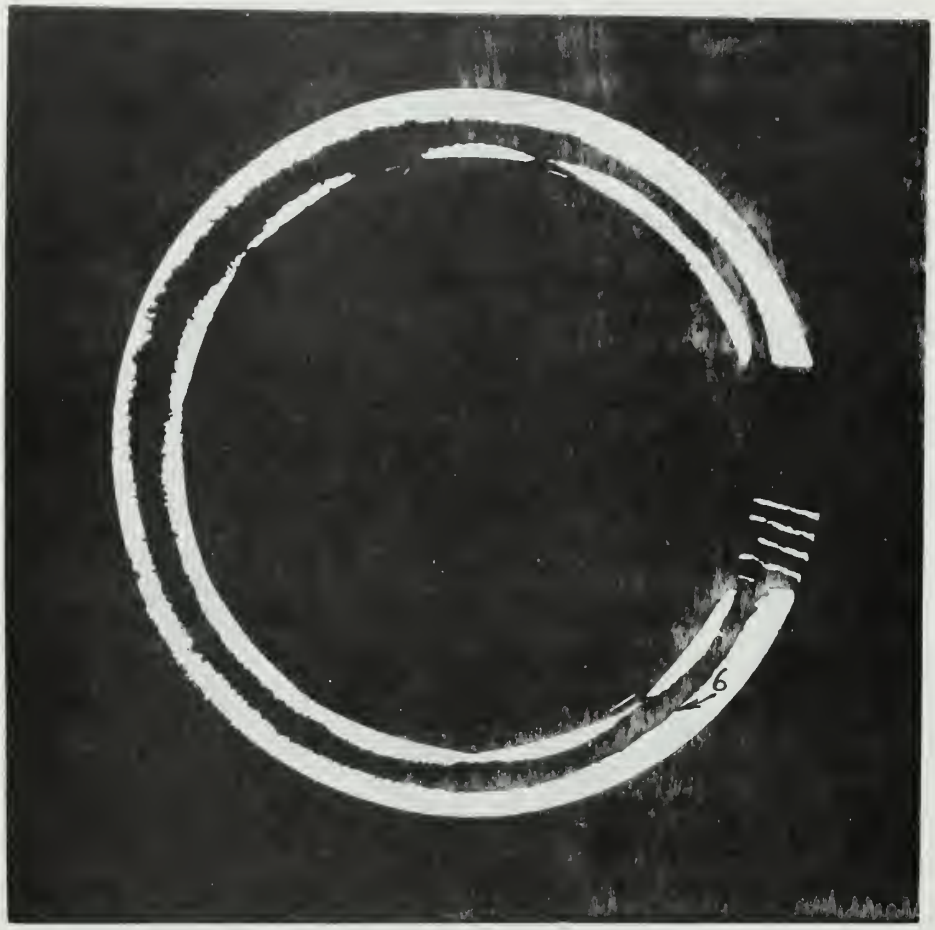

Figure 33. Model II, Slice 3. Fringe Pattern for Dark Field.

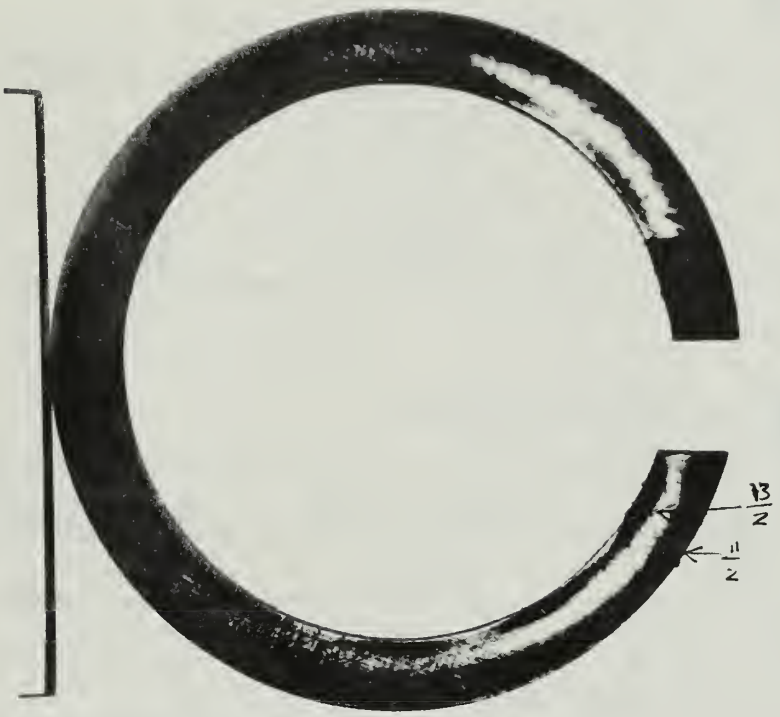
13/2
11/2

MODEL II CALCULATIONS FROM PHOTOGRAPH DATA

Slice 2

$$\frac{f}{t} = \frac{1.37}{.226} = 6.06 \text{ psi/fringe}$$

N	r, in.	$\sigma_\theta - \sigma_r$, psi	$\sigma_\theta - \sigma_r$ (Lame'), psi
2.5	1.03	15.1	20.3
3	.95	18.2	23.9
3.5	.90	21.2	26.6
4	.84	24.2	30.5
4.5	.80	27.2	33.6

Slice 3

$$\frac{f}{t} = \frac{1.37}{.202} = 6.79 \text{ psi/fringe}$$

N	r, in.	$\sigma_\theta - \sigma_r$, psi	$\sigma_\theta - \sigma_r$ (Lame'), psi
6	.85	40.7	41.4

Slice 1, zone of slice 2

N	r, in.	$\sigma_z - \sigma_r$, psi	σ_r, psi	σ_z, psi	σ_{zr}, lb/in
1	1.04	6.85	.9	5.95	6.2
1.5	.92	10.3	3.6	6.7	6.2
2	.78	13.7	8.5	5.2	4.1

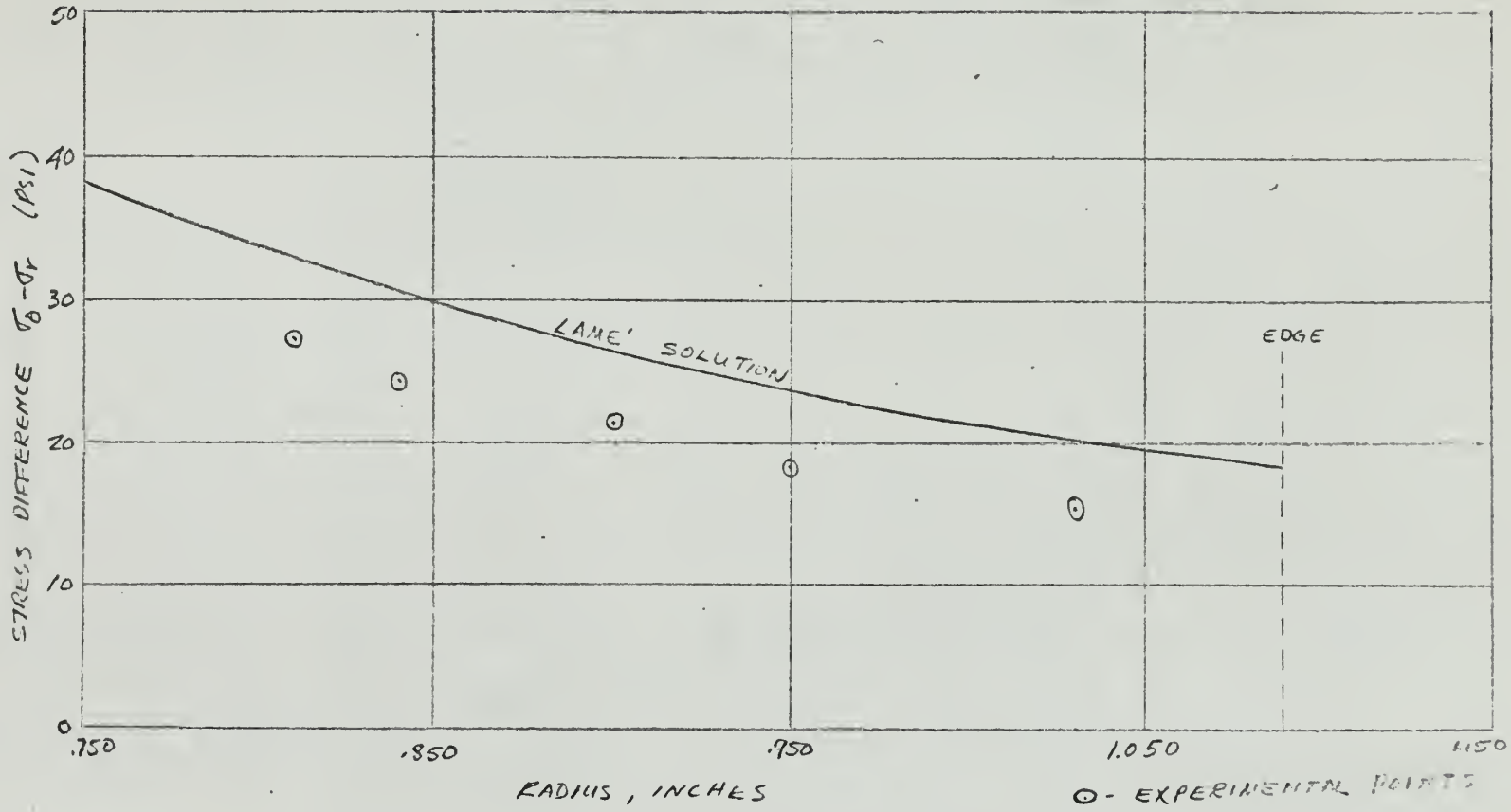

Figure 35. Model II, Slice 2. Comparison of Experimental and Theoretical Values of $\sigma_\theta - \sigma_r$.

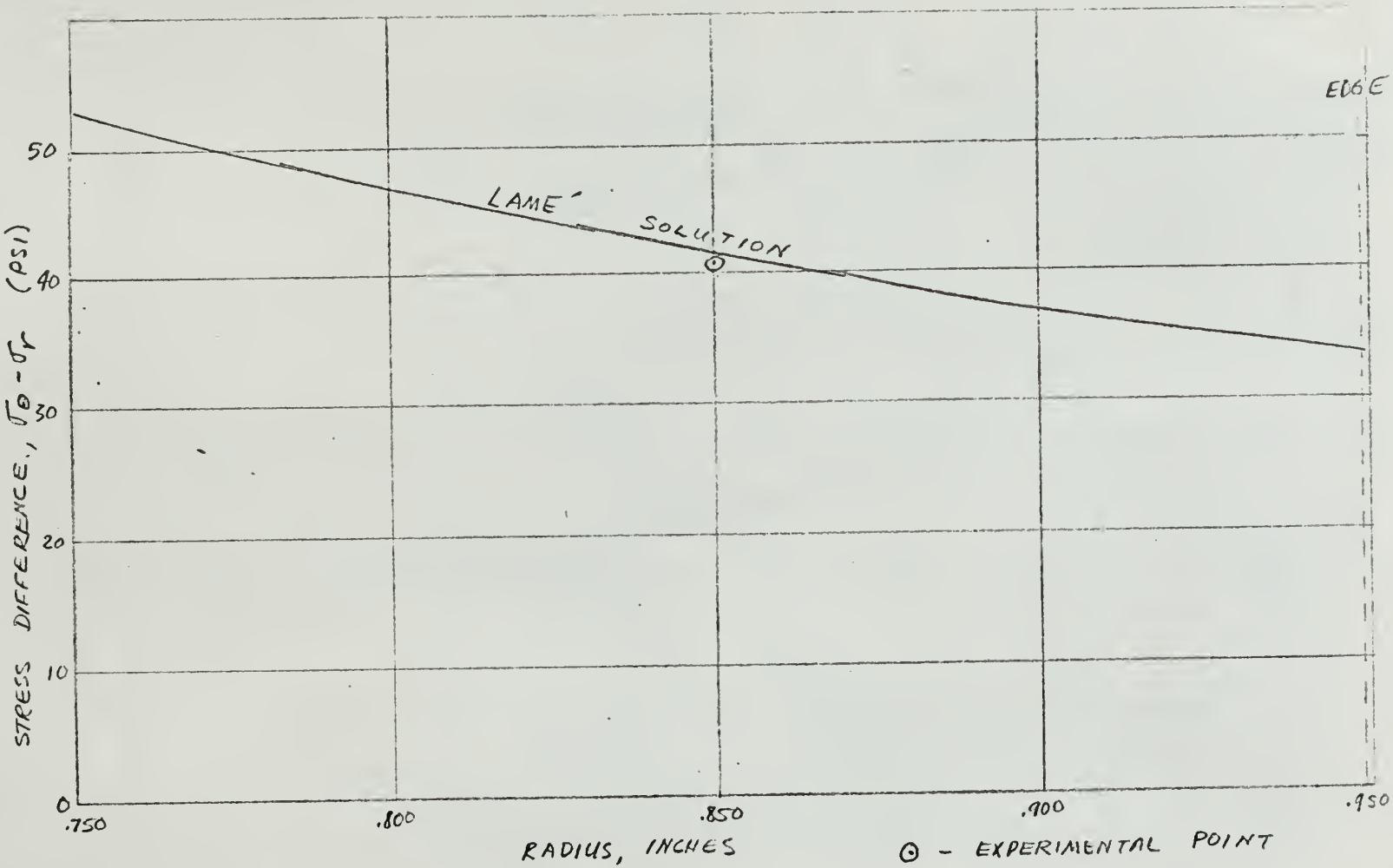

Figure 36. Model II, Slice 3. Comparison of Experimental and Theoretical Values of $\sigma_\theta - \sigma_r$.

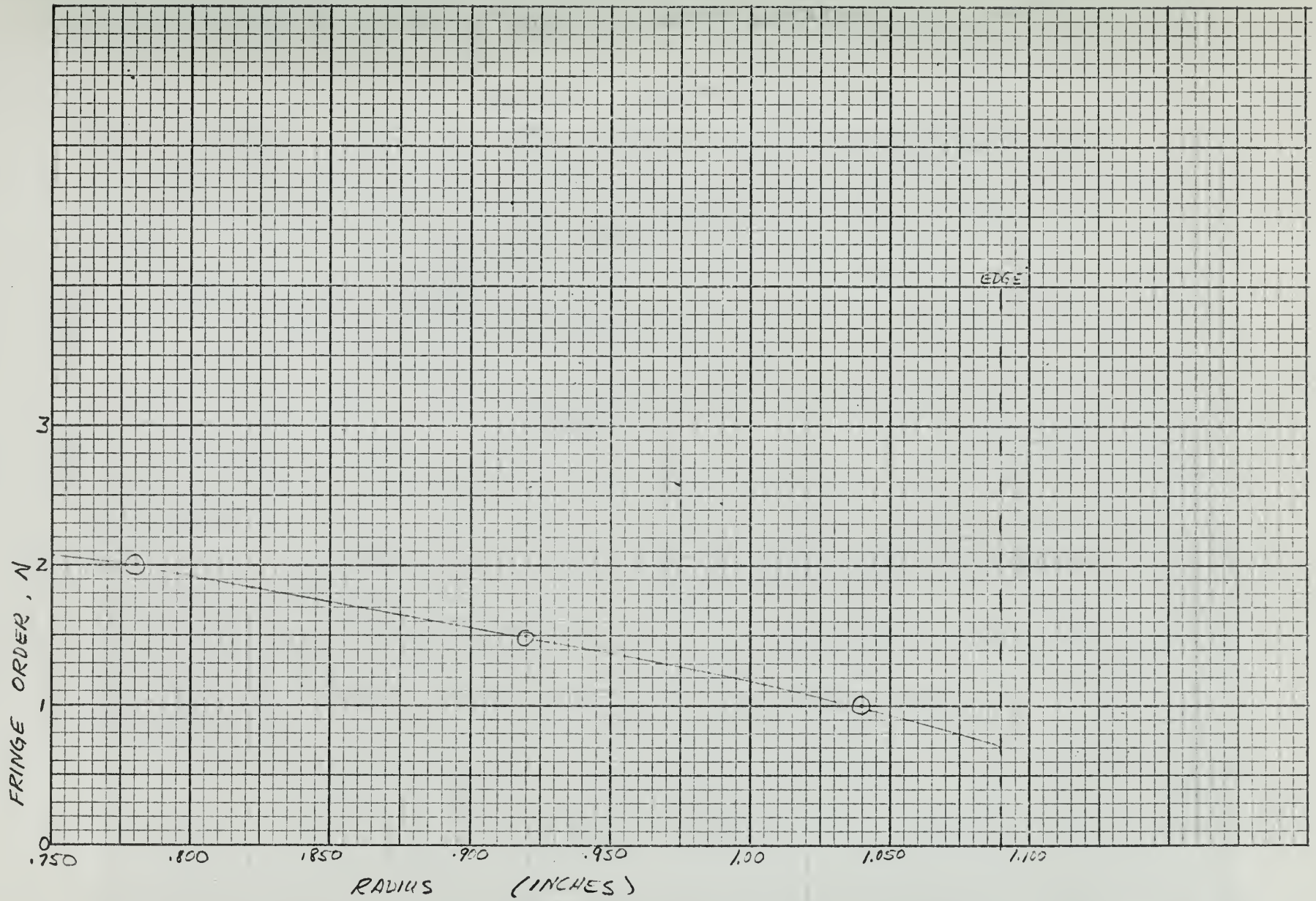

Figure 37. Model II, Slice 1. Fringe Order vs. Radius at Zone 2.

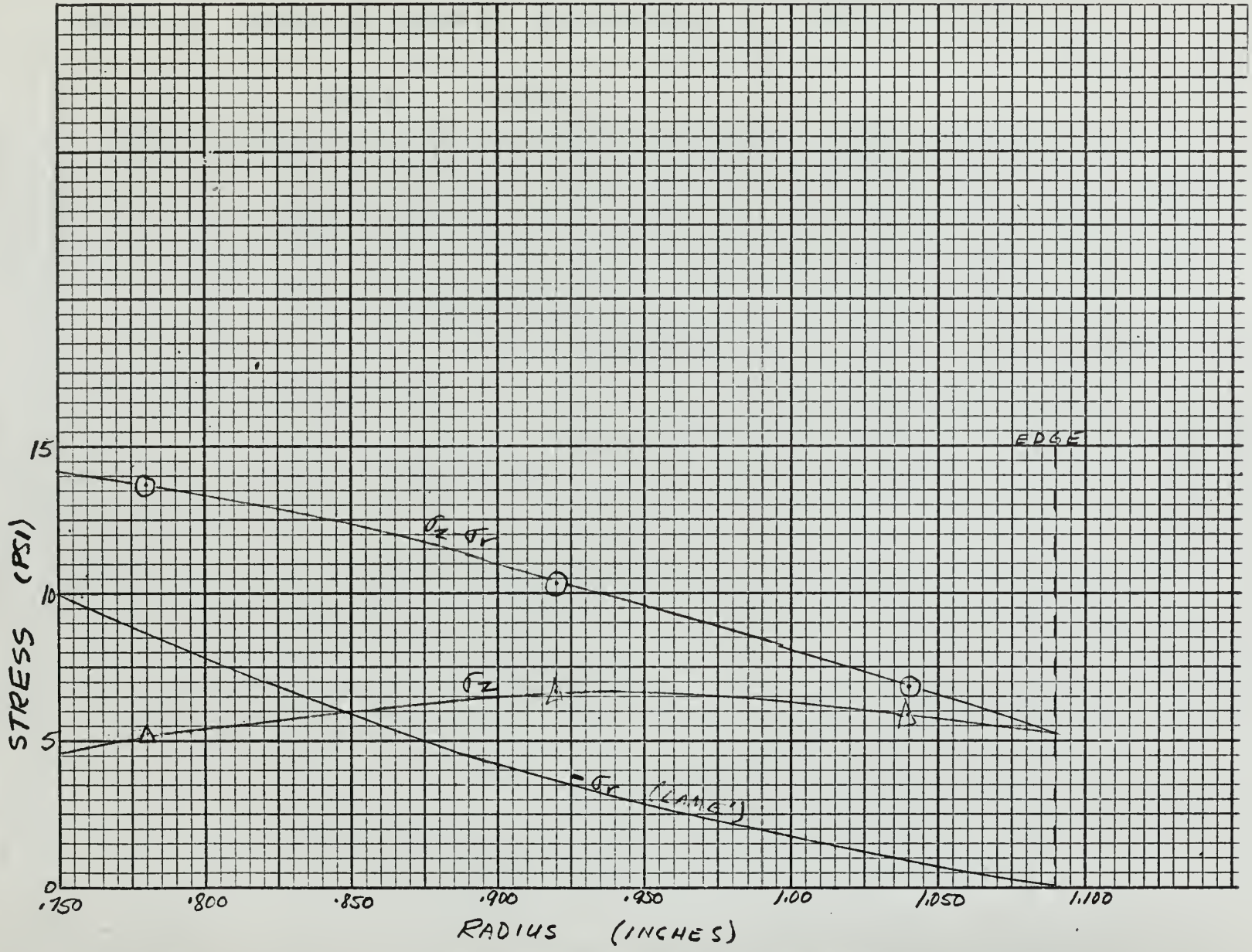

Figure 38. Model II, Slice 1. Stress Distribution at Zone 2.

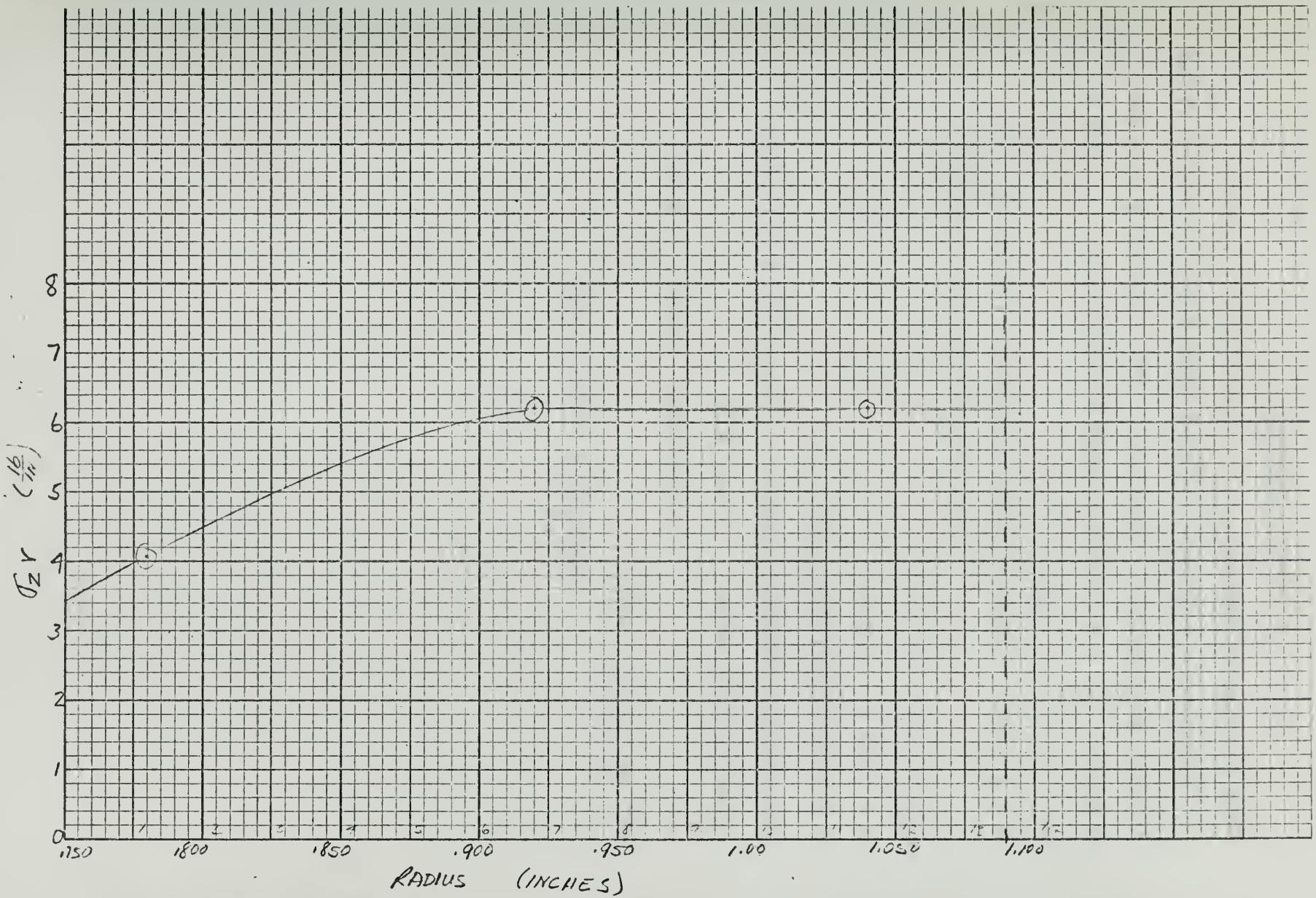

Figure 39. Model II, Slice 1. Curve for Graphical Summation at Zone 2.

MODEL II STATIC CHECK

Zone 2 (Figure 39)

Simpson's rule was applied with the abscissa divided into 14 segments 1/2 inch long. The area unit used was a square 1/2 x 1/2 inch having a scale value of .025 lb.

$A = A' - 2.48$ sq. units

$$A' = \frac{1}{3}\left[(3.4+6.2)+4(4.0+5.0+5.8+6.2+6.2+6.2+6.2) + 2(4.5+5.4+6.1+6.2+6.2+6.2)\right]$$

$A' = 76.4$ sq. units

$A = 73.9$ sq. units

$P = (73.9)(2\pi)(.025) = 11.6$ lb.

Considering internal pressure loading on the inside cross section area: $P = p_i \pi a^2$

$P = (10)(\pi)(.75)^2 = 17.3$ lb

Per cent difference:

$$\frac{11.6 - 17.3}{17.3} \times 100 = -33\%$$

APPENDIX IV

STRESS DISTRIBUTION IN THE GROOVE IN MODEL I

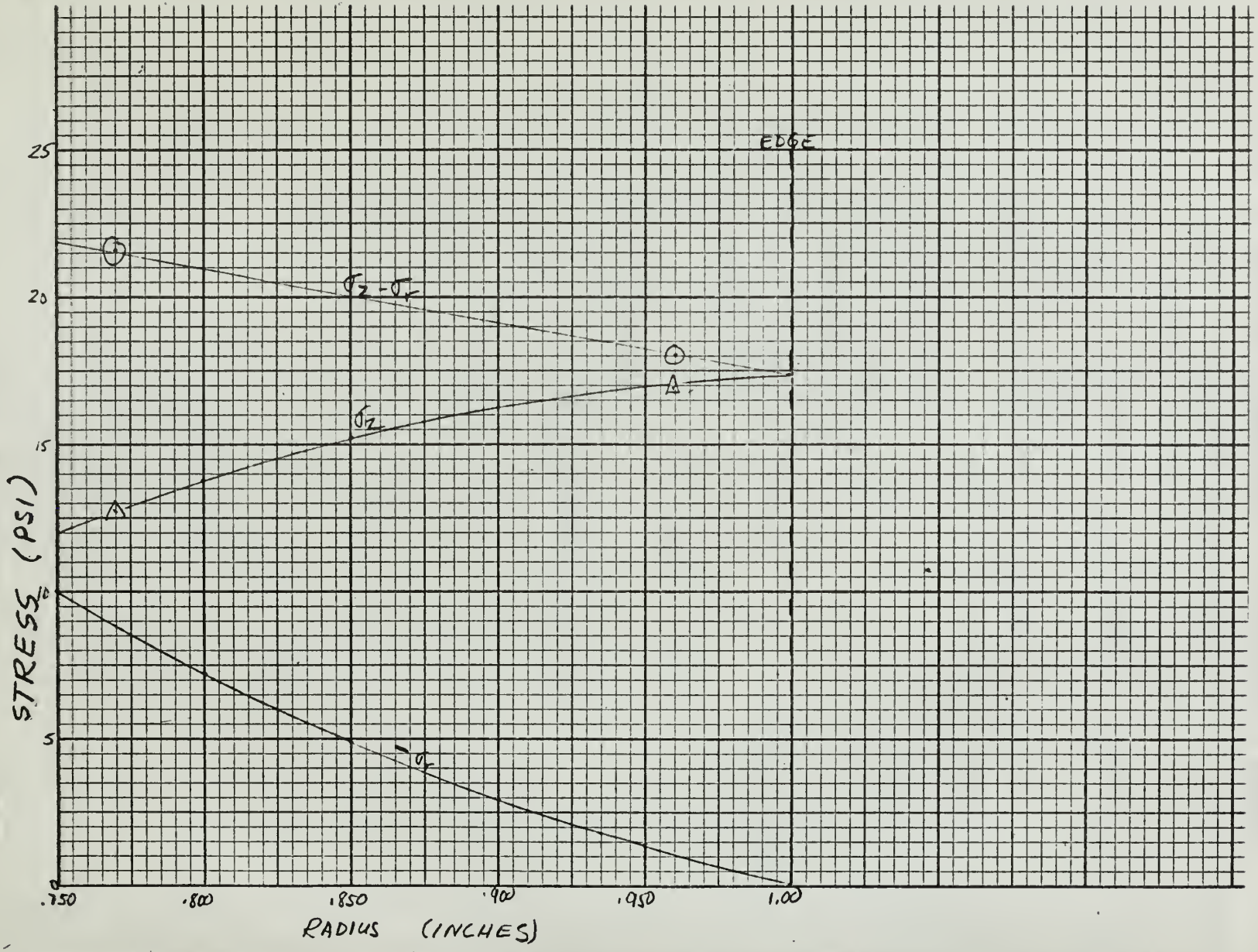

Figure 40. Model I, Slice 1. Stress Distribution at the Coupling Groove, Zone 2.

INITIAL DISTRIBUTION LIST

		No. Copies
1.	Defense Documentation Center Cameron Station Alexandria, Virginia 22314	20
2.	Library U. S. Naval Postgraduate School Monterey, California	2
3.	Naval Ship Systems Command Department of the Navy Washington, D. C. 20360	1
4.	Department of Mechanical Engineering U. S. Naval Postgraduate School Monterey, California	1
5.	Prof. Robert E. Newton Department of Mechanical Engineering U. S. Naval Postgraduate School Monterey, California	1
6.	LT Richard E. Davies, USN U. S. Naval Ship Repair Facility % FPO San Francisco, Calif. 96630	1
7.	United States Marine Engineering Laboratory Attn: Mr. Y. F. Wang, Code 832.4 Annapolis, Maryland 21402	1
8.	Lessells and Associates, Inc., 303 Bear Hill Road Waltham, Mass 02154 Attn: Dr. W. E. Cooper	1

DOCUMENT CONTROL DATA - R&D

(Security classification of title, body of abstract and indexing annotation must be entered when the overall report is classified)

1. ORIGINATING ACTIVITY *(Corporate author)*
U. S. Naval Postgraduate School
Monterey, California

2a. REPORT SECURITY CLASSIFICATION
Unclassified

2b. GROUP
N.A.

3. REPORT TITLE
A Photoelastic Investigation of Stresses in Two Different Pipe Fittings

4. DESCRIPTIVE NOTES *(Type of report and inclusive dates)*
MS Thesis - 10 January 1966 - 20 May 1966

5. AUTHOR(S) *(Last name, first name, initial)*
DAVIES, Richard E., LT, USN

6. REPORT DATE	7a. TOTAL NO. OF PAGES	7b. NO. OF REFS
May 1966	80	5

8a. CONTRACT OR GRANT NO.	9a. ORIGINATOR'S REPORT NUMBER(S)
N.A.	N.A.
b. PROJECT NO.	
c. N.A.	9b. OTHER REPORT NO(S) *(Any other numbers that may be assigned this report)*
d.	N.A.

10. AVAILABILITY/LIMITATION NOTICES
Qualified requesters may obtain copies of this report from DDC.

This document has been approved for public release and sale; its distribution is unlimited.

11. SUPPLEMENTARY NOTES	12. SPONSORING MILITARY ACTIVITY
N.A.	N.A.

Mannebach 10/9/69

13. ABSTRACT

Photoelastic methods using frozen stresses are very useful for experimentally determining stress distributions in bodies having complicated geometries for which no analytical solution is known. The method is applied to cylindrical pipe fittings having discontinuities and subjected to hydrostatic internal pressure loading. The equipment used, the method of model construct on and the calibration of the model material are described. Two models having different geometries are tested and the results are compared with theory and with each other.

DD FORM 1 JAN 64 1473

14. KEY WORDS	LINK A		LINK B		LINK C	
	ROLE	WT	ROLE	WT	ROLE	WT
Photoelastic Stress Pipe Fittings Internal pressure						

INSTRUCTIONS

1. ORIGINATING ACTIVITY: Enter the name and address of the contractor, subcontractor, grantee, Department of Defense activity or other organization *(corporate author)* issuing the report.

2a. REPORT SECURITY CLASSIFICATION: Enter the overall security classification of the report. Indicate whether "Restricted Data" is included. Marking is to be in accordance with appropriate security regulations.

2b. GROUP: Automatic downgrading is specified in DoD Directive 5200.10 and Armed Forces Industrial Manual. Enter the group number. Also, when applicable, show that optional markings have been used for Group 3 and Group 4 as authorized.

3. REPORT TITLE: Enter the complete report title in all capital letters. Titles in all cases should be unclassified. If a meaningful title cannot be selected without classification, show title classification in all capitals in parenthesis immediately following the title.

4. DESCRIPTIVE NOTES: If appropriate, enter the type of report, e.g., interim, progress, summary, annual, or final. Give the inclusive dates when a specific reporting period is covered.

5. AUTHOR(S): Enter the name(s) of author(s) as shown on or in the report. Enter last name, first name, middle initial. If military, show rank and branch of service. The name of the principal author is an absolute minimum requirement.

6. REPORT DATE: Enter the date of the report as day, month, year; or month, year. If more than one date appears on the report, use date of publication.

7a. TOTAL NUMBER OF PAGES: The total page count should follow normal pagination procedures, i.e., enter the number of pages containing information.

7b. NUMBER OF REFERENCES: Enter the total number of references cited in the report.

8a. CONTRACT OR GRANT NUMBER: If appropriate, enter the applicable number of the contract or grant under which the report was written.

8b, 8c, & 8d. PROJECT NUMBER: Enter the appropriate military department identification, such as project number, subproject number, system numbers, task number, etc.

9a. ORIGINATOR'S REPORT NUMBER(S): Enter the official report number by which the document will be identified and controlled by the originating activity. This number must be unique to this report.

9b. OTHER REPORT NUMBER(S): If the report has been assigned any other report numbers *(either by the originator or by the sponsor)*, also enter this number(s).

10. AVAILABILITY/LIMITATION NOTICES: Enter any limitations on further dissemination of the report, other than those imposed by security classification, using standard statements such as:

(1) "Qualified requesters may obtain copies of this report from DDC."

(2) "Foreign announcement and dissemination of this report by DDC is not authorized."

(3) "U. S. Government agencies may obtain copies of this report directly from DDC. Other qualified DDC users shall request through _____."

(4) "U. S. military agencies may obtain copies of this report directly from DDC. Other qualified users shall request through _____."

(5) "All distribution of this report is controlled. Qualified DDC users shall request through _____."

If the report has been furnished to the Office of Technical Services, Department of Commerce, for sale to the public, indicate this fact and enter the price, if known.

11. SUPPLEMENTARY NOTES: Use for additional explanatory notes.

12. SPONSORING MILITARY ACTIVITY: Enter the name of the departmental project office or laboratory sponsoring *(paying for)* the research and development. Include address.

13. ABSTRACT: Enter an abstract giving a brief and factual summary of the document indicative of the report, even though it may also appear elsewhere in the body of the technical report. If additional space is required, a continuation sheet shall be attached.

It is highly desirable that the abstract of classified reports be unclassified. Each paragraph of the abstract shall end with an indication of the military security classification of the information in the paragraph, represented as *(TS)*, *(S)*, *(C)*, or *(U)*.

There is no limitation on the length of the abstract. However, the suggested length is from 150 to 225 words.

14. KEY WORDS: Key words are technically meaningful terms or short phrases that characterize a report and may be used as index entries for cataloging the report. Key words must be selected so that no security classification is required. Identifiers, such as equipment model designation, trade name, military project code name, geographic location, may be used as key words but will be followed by an indication of technical context. The assignment of links, roles, and weights is optional.

DD FORM 1 JAN 64 1473 (BACK)